

Review of Sc microalloying effects in Al–Cu alloys

Shenghua Wu, Chong Yang, Peng Zhang, Hang Xue, Yihan Gao, Yuqing Wang, Ruihong Wang, Jinyu Zhang, Gang Liu, and Jun Sun

Cite this article as:

Shenghua Wu, Chong Yang, Peng Zhang, Hang Xue, Yihan Gao, Yuqing Wang, Ruihong Wang, Jinyu Zhang, Gang Liu, and Jun Sun, Review of Sc microalloying effects in Al–Cu alloys, *Int. J. Miner. Metall. Mater.*, 31(2024), No. 5, pp. 1098-1114. <https://doi.org/10.1007/s12613-024-2841-8>

View the article online at [SpringerLink](#) or [IJMMM Webpage](#).

Articles you may be interested in

Chong-yu Liu, Guang-biao Teng, Zong-yi Ma, Li-li Wei, Bing Zhang, and Yong Chen, [Effects of Sc and Zr microalloying on the microstructure and mechanical properties of high Cu content 7xxx Al alloy](#), *Int. J. Miner. Metall. Mater.*, 26(2019), No. 12, pp. 1559-1569. <https://doi.org/10.1007/s12613-019-1840-7>

Yu-ting Wu, Chong Li, Ye-fan Li, Jing Wu, Xing-chuan Xia, and Yong-chang Liu, [Effects of heat treatment on the microstructure and mechanical properties of Ni₃Al-based superalloys: A review](#), *Int. J. Miner. Metall. Mater.*, 28(2021), No. 4, pp. 553-566. <https://doi.org/10.1007/s12613-020-2177-y>

Surajit Basak, Prosanta Biswas, Surajit Patra, Himadri Roy, and Manas Kumar Mondal, [Effect of TiB₂ and Al₃Ti on the microstructure, mechanical properties and fracture behaviour of near eutectic Al–12.6Si alloy](#), *Int. J. Miner. Metall. Mater.*, 28(2021), No. 7, pp. 1174-1185. <https://doi.org/10.1007/s12613-020-2070-8>

Zhi-hao Zhang, Jie Xue, Yan-bin Jiang, and Feng Jin, [Effect of pre-annealing treatment on the microstructure and mechanical properties of extruded Al–Zn–Mg–Cu alloy bars](#), *Int. J. Miner. Metall. Mater.*, 24(2017), No. 11, pp. 1284-1292. <https://doi.org/10.1007/s12613-017-1521-3>

Zheng-hua Deng, Hai-qing Yin, Xue Jiang, Cong Zhang, Guo-fei Zhang, Bin Xu, Guo-qiang Yang, Tong Zhang, Mao Wu, and Xuan-hui Qu, [Machine-learning-assisted prediction of the mechanical properties of Cu–Al alloy](#), *Int. J. Miner. Metall. Mater.*, 27(2020), No. 3, pp. 362-373. <https://doi.org/10.1007/s12613-019-1894-6>

Li Lin, Bao-shun Li, Guo-ming Zhu, Yong-lin Kang, and Ren-dong Liu, [Effects of Nb on the microstructure and mechanical properties of 38MnB5 steel](#), *Int. J. Miner. Metall. Mater.*, 25(2018), No. 10, pp. 1181-1190. <https://doi.org/10.1007/s12613-018-1670-z>


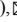


IJMMM WeChat



QQ author group

Review of Sc microalloying effects in Al–Cu alloys

Shenghua Wu¹, Chong Yang¹, Peng Zhang¹, Hang Xue¹, Yihan Gao^{1,3}, Yuqing Wang¹, Ruihong Wang², Jinyu Zhang¹, Gang Liu¹,, and Jun Sun¹,

1) State Key Laboratory for Mechanical Behavior of Materials, Xi'an Jiaotong University, Xi'an 710049, China

2) School of Materials Science and Engineering, Xi'an University of Technology, Xi'an 710048, China

3) School of Aerospace Engineering, North University of China, Taiyuan 030051, China

(Received: 20 September 2023; revised: 25 January 2024; accepted: 29 January 2024)

Abstract: Artificially controlling the solid-state precipitation in aluminum (Al) alloys is an efficient way to achieve well-performed properties, and the microalloying strategy is the most frequently adopted method for such a purpose. In this paper, recent advances in length-scale-dependent scandium (Sc) microalloying effects in Al–Cu model alloys are reviewed. In coarse-grained Al–Cu alloys, the Sc-aided Cu/Sc/vacancies complexes that act as heterogeneous nuclei and Sc segregation at the θ' -Al₂Cu/matrix interface that reduces interfacial energy contribute significantly to θ' precipitation. By grain size refinement to the fine/ultrafine-grained scale, the strongly bonded Cu/Sc/vacancies complexes inhibit Cu and vacancy diffusing toward grain boundaries, promoting the desired intragranular θ' precipitation. At nanocrystalline scale, the applied high strain producing high-density vacancies results in the formation of a large quantity of (Cu, Sc, vacancy)-rich atomic complexes with high thermal stability, outstandingly improving the strength/ductility synergy and preventing the intractable low-temperature precipitation. This review recommends the use of microalloying technology to modify the precipitation behaviors toward better combined mechanical properties and thermal stability in Al alloys.

Keywords: aluminum alloy; microalloying effect; length-scale dependence; precipitation; mechanical properties

1. Introduction

Due to its appealing high strength and low density, the materials community has shown much interest in Al alloys. Heat-treatable Al–Cu alloys are the most typical precipitation strengthening Al alloys because they offer the basis for different types of age-hardening Al alloys. The commonly observed precipitation sequence during the aging of Al–Cu alloys is supersaturated solid solution (SSSS) → Guinier–Preston (GP) zones → θ'' → θ' → θ , which often serves as a template to describe the fundamentals of precipitation from supersaturated solution and precipitation hardening [1].

Age hardening of heat-treatable Al alloys is mainly caused by the decomposition of excess alloying elements into nanosized precipitates, which act as effective obstacles to moving dislocations [2]. The classical nucleation theory has been extensively adopted to quantitatively determine the critical radius of a nucleus [3–5]. The nucleation rate is normally described by the classical nucleation rate equation [6]. The subsequent growth rate of precipitates in heat-treatable Al alloys depends on the shape, composition, and interfacial structure [2,7] and can be quantitatively expressed by the Lifshitz–Slyozov–Wagner model modified by Boyd and Nicholson [8]. The strengthening effects of precipitates closely depend on size, volume fraction, interparticle spacing, and character-

istics [9–10], all of which are determined by composition, processing technology, and heat treatment [11–13]. The composition–processing–microstructure–property relationships can be well presented in heat-treatable Al alloys. Generally, artificial aging is applied to control the precipitation behaviors of heat-treatable Al alloys, such as nucleation and growth kinetics of precipitates [14]. In the past three decades, dynamic age-hardening models that quantitatively predict the variation in precipitate parameters with aging treatments (temperature and time, based on the precipitation thermodynamic and kinetic theories) and the associated strength evolution (stemming from the precipitate–dislocation interactions) have been well established [9,11,15–18]. Significant advances in quantitative prediction of the precipitation hardening of heat-treatable Al alloys greatly move forward the development of high-performance Al alloys.

In addition to optimization of aging technologies, microalloying has also been effectively employed in controlling the precipitation in Al alloys [19–21], i.e., controlling the precipitate size and distribution by adding small amounts of microalloying elements. In general, the microalloying mechanisms in Al alloys can be categorized into two groups: promoting the precipitation of hardening particles that are inherently precipitated in Al alloys and forming additionally introduced new precipitates [22]. The first mechan-

 Corresponding authors: Gang Liu E-mail: lgsammer@xjtu.edu.cn; Jun Sun E-mail: junsun@xjtu.edu.cn

© University of Science and Technology Beijing 2024

ism has been widely explored in Al–Cu alloys [23–30]. The possible mechanisms include (i) heterogeneous nucleation mechanism [23–28,31–32] and (ii) interfacial segregation mechanism [29–30]. In the first mechanism, atom probe field ion microscopy demonstrated this in the Sn (Cd or In)-microalloyed Al–Cu alloy [31], in which the microalloying atoms can be heterogeneous nucleation sites for θ' precipitates. In the second mechanism, the microalloying atoms significantly influence the interfacial conditions (e.g., interface structures, chemistry composition, and energies), modifying the subsequent precipitation behaviors and hardening response, such as precipitation nucleation, number density, and driving force for precipitate coarsening. This can reduce the interfacial energy, which can be quantitatively expressed by following the proposed thermodynamic methods [29–30], benefiting greatly from the advances in atom probe tomography (APT) [33–34].

During the aging precipitation in heat-treatable Al alloys, atomic diffusion determines the precipitation kinetics, where vacancies can fasten the diffusion of substitutional alloying elements. Rapid quenching from solution treatment [35–37] or plastic deformation [38–39] can produce excess vacancies in Al alloys. The vacancy–microalloying element interaction can be applied to significantly adjust the precipitation behaviors. Hardy [23] reported that In-, Sn-, or Cd-microalloyed Al–Cu alloys showed suppressed natural aging, while aging at elevated temperatures resulted in improved precipitation. The strong binding between microalloying elements (In, Sn, or Cd) and vacancies prevents the quenched vacancies from accelerating Cu diffusion greatly during storage in ambient conditions. However, higher temperatures can free the vacancies from the solute–vacancy complexes, which promotes θ' precipitation. Similar precipitation behaviors have also been found in Sn-microalloyed Al–Mg–Si alloys [40], effectively easing the deleterious natural aging in Al–Mg–Si alloys. In addition, experimental and simulation research disclosed that one vacancy can contribute to the formation of up to 10 clusters, transferring about 1000 atoms to clusters, which can be considered precursors of precipitates [41]. Atomic-resolution Cs-corrected scanning transmission electron microscopy (TEM) and APT show that high-density vacancies (stimulated at the free surface by heating) led to promoted precipitation, while a lack of vacancies (annihilated at the free surface by thinning) led to suppressed precipitation, both in small-sized samples [4,42]. Recent studies reported that reducing the crystalline size in supersaturated Al–Mg and Al–Zn alloys to an extremely small size (~8 and 9 nm, respectively) can completely inhibit the diffusion-controlled Al_3Mg_2 precipitation and the spinodal decomposition of Zn-rich particles from supersaturated nanograins, which are related to the quite low vacancy concentration in nanograins [43–44]. During the precipitation process, excess vacancies can also reduce the nucleation energy barrier by releasing the misfit strain of the nucleus [4]. In general, annihilation of excess vacancies at grain boundaries forms precipitate-free zones near grain boundaries in Al alloys [45–46]. All the pre-

vious works exclusively point to the same conclusion that vacancies play crucial roles in affecting the precipitation in Al alloys.

Due to the ability of refining grain size down into nanometer scale, extensive researches have been conducted on severe plastic deformation (SPD, e.g., high-pressure torsion (HPT) and equal-channel angular pressing (ECAP)), aiming at fabricating high-strength Al alloys with refined grains [47–52]. In general, after SPD processing, a large quantity of crystal defects is present in the as-deformed Al alloys, such as nonequilibrium grain boundaries, dislocations, and vacancies, due to the applied high strain [49,53]. The precipitation behaviors in heat-treatable Al alloys strongly depend on the initial microstructure [54–57]. With submicron- and nanometer-scale grain size, much faster precipitation takes place (at a rate of one to several orders of magnitude faster) compared with coarse-grained (CG) counterparts [54–55]. The deformation-introduced high-density crystal defects significantly accelerate the solute diffusion toward high-energy dislocations and grain boundaries, where low-temperature precipitation occurs. In SPD-processed Al–Cu alloys with nanosized grains, extensive intergranular equilibrium θ - Al_2Cu precipitates rather than intragranular metastable θ' - Al_2Cu can form even during storage in ambient conditions [54]. Similarly, after SPD processing in Al–Zn–Mg–Cu alloy, equilibrium phases were found to precipitate at grain boundaries [55], indicating that precipitation behaviors are length-scale dependent in Al alloys, and there are excellent variations in the size, chemistry, and spatial distribution of precipitates with reducing grain size. Low-temperature preferential precipitation at grain boundaries in Al alloys with submicron and nanosized grains is catastrophic for subsequent age hardening, for which lower solute supersaturation in the matrix is insufficient for intragranular precipitation. Furthermore, the intergranular precipitates introduce stress concentrations at the grain boundaries and tend to localize strain and cracking near them, resulting in intergranular fracture and unresolved low ductility [53,58]. The intractable low-temperature precipitation and low ductility largely limit practical application of high-strength Al alloys with submicron and nanosized grains. Extensive research proved that microalloying effects are efficient at modifying precipitation behaviors and thus significantly endowing mechanical properties. However, a vast majority of studies on microalloying have mainly concentrated on CG Al alloys, and the microalloying effects at different length scales in Al alloys remain under debate. Thus, developing an intelligent microalloying strategy for improved thermal stability and ductility of high-strength Al alloys with submicron and nanosized grains is the usual direction.

Scandium (Sc), as the most efficient microalloying element per atomic fraction added imparting on precipitation behaviors, has been extensively applied in Al alloys [59–60]. Sc addition in pure Al can form Al_3Sc nanoprecipitates with L1_2 structure (with sizes from several nanometers to tens of nanometers) [59]. Aging treatment and Sc content can signi-

ificantly influence the size and morphology of Al_3Sc precipitates [61–62]. High-density Al_3Sc precipitates can contribute significantly to strengthening, for which the strengthening effects have been quantitatively modeled [62]. Also, their high thermal stability at high temperatures (due to the slow diffusivity of Sc in the Al matrix) allows their wide utility in high-temperature services, such as automotive engines and aircraft [62–63]. To further improve performance at high temperatures, a series of Al–Sc-based alloys (microalloyed by Zr, Er, Ti, etc.) with a well-performed creep resistance have been developed, for which the better creep resistance is related to the typical core–shell structure of precipitates [64–67]. The element with a larger diffusivity forms the core first, and then the element with a lower diffusivity segregates to form the shell. In recent years, in additively manufactured Al alloys, Sc in minor amount is added to form Al_3Sc -based particles that serve as heterogeneous nuclei for grains, producing equiaxed fine grains to inhibit hot crack during printing [68–69]. In Sc-microalloyed Al–Mg alloys [70–71], Mg solutes were found to both segregate at the coherent $\text{Al}_3\text{Sc}/\text{Al}$ matrix interface and be located at the centers of Al_3Sc precipitates (the diffusivity of Mg in Al_3Sc was approximately seven orders of magnitude slower than that in pure Al at 300°C), which simultaneously decreases the growth/coarsening rate of Al_3Sc precipitates and improves the creep resistance. A combined Sc and Zr addition in Al–Zn–Mg–Cu alloys can result in the formation of $\text{Al}_3(\text{Sc}_x\text{Zr}_{1-x})$ particles, pinning subgrain and grain boundaries during heat treatment to inhibit recrystallization and precipitate-free zone, improving both corrosion resistance and strength [60,72–74]. However, adding minor Sc in Al alloys is not always advantageous to the precipitation and mechanical performance. For instance, adding 0.32wt% Sc in an Al–Cu–Mg–Ag alloy degrades the yield strength compared with the Sc-free counterpart [75], which is due to the formation of coarse $\text{Al}_8\text{Cu}_4\text{Sc}$ intermetallic particles, lowering the amount of Cu atoms available for the strengthening Ω precipitates. In Sc-microalloyed Al–Mg–Si alloy [76], the formation of strong Si–Sc pairs (with a high negative enthalpy of $\sim -207 \text{ kJ}\cdot\text{mol}^{-1}$) and weak Mg–Sc pairs (with an enthalpy of $\sim -13 \text{ kJ}\cdot\text{mol}^{-1}$) lowered the diffusivity of Si and Mg solutes, thus reducing the growth rate of the strengthening β'' precipitates.

With the development of Sc microalloying technology, Sc-microalloyed Al alloys have received much attention, aiming at artificially controlling precipitation behaviors (including the size, chemistry, interfacial characteristics, and spatial distribution of precipitates) and resultantly improving mechanical properties [39,53,58,77–82]. This paper presents a review of the length-scale dependent Sc microalloying effects on defect structures, precipitation behaviors, and mechanical properties in Al–Cu alloys. From both materials science and mechanics perspectives, the principles and lessons learned from the relatively simple model Sc-microalloyed Al–Cu alloy can elaborate on the design strategy of microalloying to change precipitation behaviors and enhance the mechanical properties in other Al alloys.

2. Precipitation in Al–Cu alloys

Fig. 1 illustrates the binary Al–Cu phase diagram at the Al-rich side. The single-phase supersaturated solid solution at high temperatures can decompose into θ , θ' , θ'' , and GP zones in sequence with decreasing temperature [83]. GP zones are composed of single Cu layers in the Al matrix (Fig. 2(a)), which are coherent with the matrix. GP zones of the lowest interfacial energy and nucleation energy barrier are commonly formed at low-temperature aging ($<160^\circ\text{C}$) or during natural aging [83]. The θ'' phase includes two Cu atom layers separated by three Al atom layers and is essentially of a distorted face centered cubic structure (with a nominal composition of Al_3Cu , Fig. 2(b)). The θ'' phase can form directly by decomposition of supersaturated solution or the transformation of GP zones. The metastable θ' phase contributes the most to the strengthening of Al–Cu alloys. The θ' phase has a tetragonal structure (space group $14/mmm$, $a = 0.404 \text{ nm}$, $c = 0.580 \text{ nm}$, Fig. 2(c)) with a nominal composition of Al_2Cu . The large structural discrepancy between θ' and Al matrix (face centered cubic, $a = 0.404 \text{ nm}$) introduces additional interfacial energy and strain energy, which, based on the classic nucleation theory, increases the nucleation energy barrier. Heterogeneous nucleation sites, such as defects (e.g., dislocations, interfaces, grain boundaries) and pre-existing particles, are usually needed for the nucleation of the θ' phase. The equilibrium θ phase has a stoichiometric composition close to Al_2Cu and with a complex body-centered tetragonal structure (space group $14/mcm$, $a = 0.607 \text{ nm}$, $c = 0.487 \text{ nm}$, Fig. 2(d)). The θ phase is incoherent with the matrix, and various orientation relationships between θ phase and matrix have been reported, which results in various morpho-

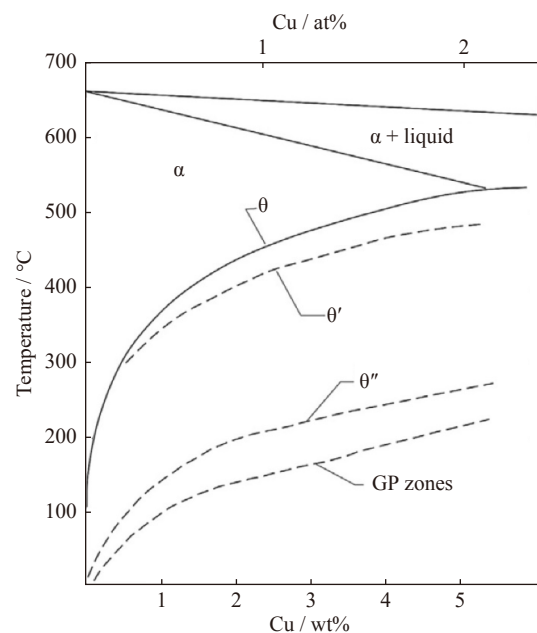


Fig. 1. Al-rich side of the Al–Cu binary phase diagram [83]. Reprinted from *Physical Metallurgy*, J.F. Nie, *Physical metallurgy of light alloys*, 2009-2156, Copyright 2014, with permission from Elsevier.

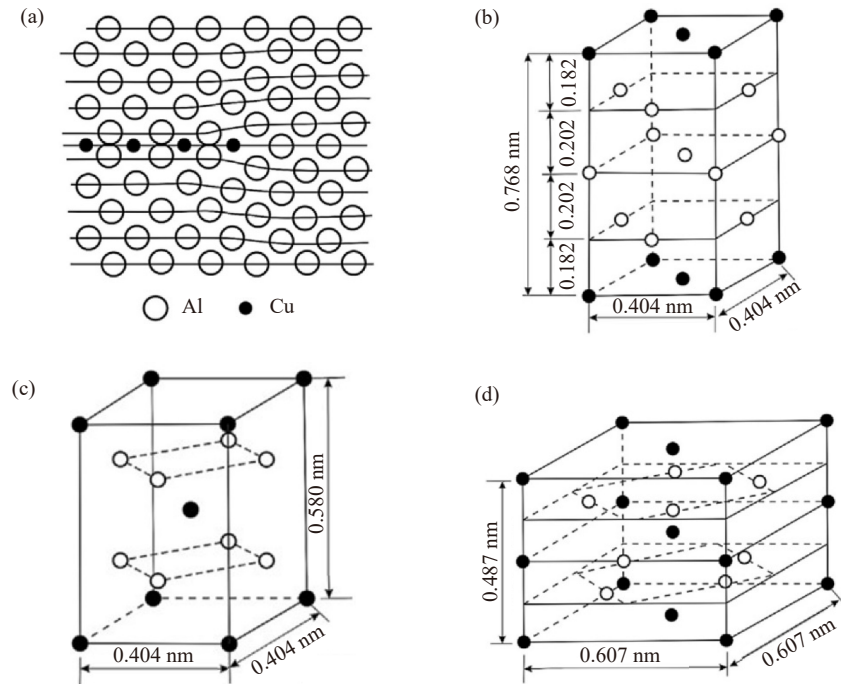


Fig. 2. Precipitate structure in Al–Cu alloys [83]: (a) GP zone; (b) θ'' unit cell; (c) θ' unit cell; (d) θ unit cell. Reprinted from *Physical Metallurgy*, J.F. Nie, *Physical metallurgy of light alloys*, 2009-2156, Copyright 2014, with permission from Elsevier.

logy shapes. Although the driving force for θ phase precipitation is the largest, the highest nucleation energy barrier originating from the complete incoherence with the matrix makes the equilibrium θ phase the most difficult to precipitate.

In-depth investigations have been performed to explore the microalloying effects on the precipitation behaviors and mechanical properties of Al–Cu alloys [5,24–26,29–30,84–87]. Minor Sn addition in Al–Cu alloys led to the formation of Sn clusters in the as-quenched state [26], which transformed into β -Sn particles during the artificial aging. The β -Sn particles served as the heterogeneous nucleation sites for θ' precipitates [24–25], enhancing the precipitation behaviors. Minor Mg and Si solutes were found to segregate at both the coherent and semicoherent θ' /matrix interface, reducing the interfacial energy and thus increasing the nucleation current [29–30]. In the Al–Cu–Ag alloy, a Ag-rich bilayer was formed at the interface and acted as a barrier to Cu diffusion [84]. The lateral growth of θ' precipitates was at the expense of neighboring γ' (AlAg_2) precipitates to supply Ag atoms, which existed before the θ' precipitation. Minor Au addition could reduce the nucleation energy barrier of θ' precipitation and substitute the Cu atoms in the θ' precipitates to form agglomerated Au clusters [5,86], resulting in an improved age-hardening response. Interestingly, a novel sandwich structure could be formed (the separation between the coherent interface of the θ' precipitate and its adjacent GP zone is always three $\{002\}_{\text{Al}}$ planes).

3. Coarse-grained Al–Cu alloys with Sc microalloying

Minor Sc addition in Al alloys can introduce the forma-

tion of primary Al_3Sc intermetallic particles [59,88], Al_3Sc dispersoids [89–90], and Sc clusters [64], in addition to Al_3Sc precipitates (Fig. 3) during different heat treatment stages. In artificial aging, the main strengthening phase in Al–Cu alloys

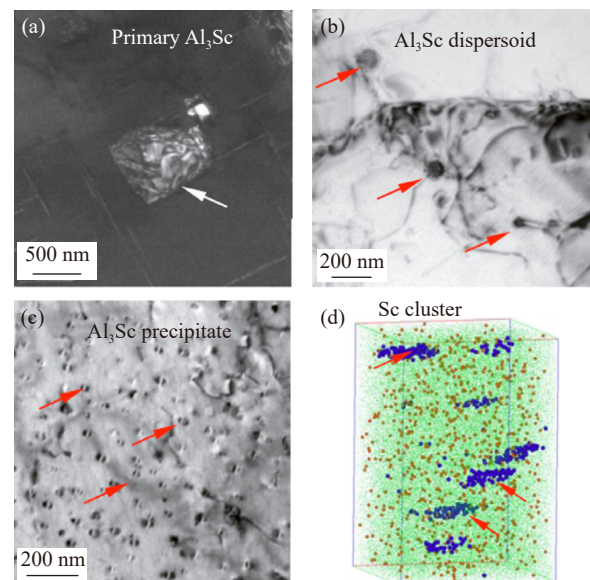


Fig. 3. Typical TEM images and APT map of Al_3Sc particles and Sc-rich clusters (marked by arrows) in Al alloys [78]: (a) primary Al_3Sc particles with a size of several micrometers; (b) Al_3Sc dispersoids with a size of tens of nanometers; (c) Al_3Sc precipitates with a size of several nanometers; (d) Sc-rich clusters (green: Al atoms; orange: Cu atoms; blue: Sc atoms; dimensions: $20 \text{ nm} \times 20 \text{ nm} \times 30 \text{ nm}$). Reprinted from *Acta Mater.*, Vol. 61, B.A. Chen, G. Liu, R.H. Wang, et al., *Effect of interfacial solute segregation on ductile fracture of Al–Cu–Sc alloys*, 1676-1690, Copyright 2013, with permission from Elsevier.

loys is the shear-resistant plate-like θ' precipitates [91], comprising of broad coherent and narrow semicoherent interfaces with the matrix [92–93]. The interaction and synergy between the main alloying element Cu and microalloying element Sc in Al–Cu–Sc alloys mediated by heat treatment and vacancies can be strategically manipulated to artificially control precipitation behaviors and improve mechanical properties.

After homogenization and solution heat treatment, Al_3Sc dispersoids with a size of tens of nanometers can be introduced in Al–Cu–Sc alloys. Yang *et al.* [94] prepared Al– $X\text{Cu}$ –0.3wt%Sc alloys ($X = 0\text{wt}\%$, 1.0wt%, 1.5wt%, and 2.5wt%), systematically examining the effect of Cu content on the formation of Al_3Sc dispersoids after solution heat treatment, and found that increasing Cu content can suppress the formation of Al_3Sc dispersoids, i.e., the size and volume fraction of Al_3Sc dispersoids were both reduced with the added Cu content. Based on the interaction between the main alloying element Cu and microalloying element Sc, the possible underlying mechanism was that Cu promotes the solid solubility of Sc in the Al matrix, reducing the supersaturation and available Sc atoms for the growth of Al_3Sc dispersoids. At 2.5wt% Cu, more Sc atoms were dissolved into the matrix, thus avoiding Al_3Sc dispersoid growth. Subsequently aging at 250°C for 8 h, a higher Cu content led to a more promoted θ' precipitation in the Al–Cu–Sc alloys. Fig. 4 compares that a more significant Sc microalloying effect can be found in the Al–2.5Cu–0.3Sc alloy, i.e., the precipitate radius reduction and number density increment were the largest compared with those of the Sc-free Al–2.5Cu alloy. APT results shown in Fig. 5 revealed that the aged Al–2.5Cu–0.3Sc alloy has a higher interfacial Sc segregation ($\sim 0.8\text{at}\%$) than the aged Al–1.5Cu–0.3Sc alloy ($\sim 0.3\text{at}\%$). Sc-promoted θ' precipitation was mainly related to two factors: (i) the Sc-

aided formation of complex Cu/Sc/vacancy clusters as preferential nucleation sites for θ' precipitates; (ii) Sc segregation at the θ' /matrix interface (reducing the interfacial energy and preventing Cu atoms from diffusing across the interface [29–30,95]) that inhibits precipitate growth [30,78]. Therefore, the higher remaining dissolved Sc atoms in the matrix induced by a higher Cu content contributed more to the θ' precipitation during subsequent aging. The room-temperature tensile results in Fig. 6(a) and (b) demonstrated that the aged Al–2.5Cu–0.3Sc alloy has the highest strength, which is in agreement with the microstructural observations (i.e., the more refined precipitate size and higher number density). However, due to the formation of larger-sized Al_3Sc dispersoids, where cracks are easier to initiate and propagate, the Sc-added Al–Cu alloys had less ductility. Due to the higher interfacial Sc segregation that inhibits precipitate coarsening, the Al–2.5Cu–0.3Sc alloy had the highest tensile strength at 300°C (~ 200 MPa) while sacrificing no high-temperature ductility (Fig. 6(c) and (d)), indicating that Sc segregation at the θ' /matrix interface shows promise in improving the resistance of precipitates to high-temperature coarsening. Improving the coarsening resistance of θ' precipitates by interfacial Sc segregation is similar to the works of Seidman *et al.* [65,67,96], who employed elements with slower diffusivity (e.g., Zr, Ti) to segregate at the $\text{Al}_3\text{Sc}/\text{Al}$ interface. Such an inert protected shell acted as a barrier to the diffusion of solutes.

In addition to Cu content dependence, Sc segregation effects showed a non-monotonic aging temperature dependence [77–78]. In the Al–2.5Cu–0.3Sc alloy, the strongest interfacial Sc segregation occurred at 250°C aging ($\sim 0.8\text{at}\%$) compared with 200°C ($\sim 0.22\text{at}\%$) and 300°C ($\sim 0.28\text{at}\%$) aging. The underlying mechanism behind such a discrepancy was the limited diffusion of Sc atoms at 200°C [61] and

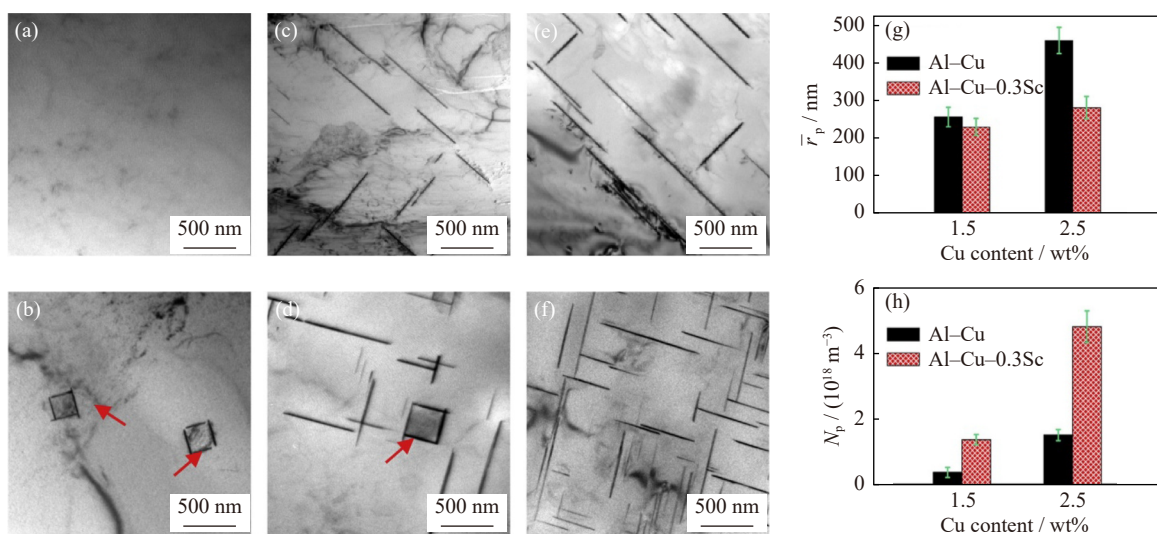


Fig. 4. Typical TEM images and corresponding statistical results of the size and distribution of θ' precipitates in Al– $X\text{Cu}$ ((a) 1.0wt% Cu; (c) 1.5wt% Cu; (e) 2.5wt% Cu) and Al– $X\text{Cu}$ –Sc ((b): 1.0wt% Cu; (d) 1.5wt% Cu; (f) 2.5wt% Cu) after 250°C aging for 8 h. (g, h) Effects of Cu content and Sc addition on the average radius (\bar{r}_p) and number density (N_p) of the θ' precipitate. The arrows in (b, d) indicate that the θ' precipitates nucleate heterogeneously on the Al_3Sc dispersoid [94]. Reprinted from *Acta Mater.*, Vol. 119, C. Yang, P. Zhang, D. Shao, *et al.*, The influence of Sc solute partitioning on the microalloying effect and mechanical properties of Al–Cu alloys with minor Sc addition, 68–79, Copyright 2016, with permission from Elsevier.

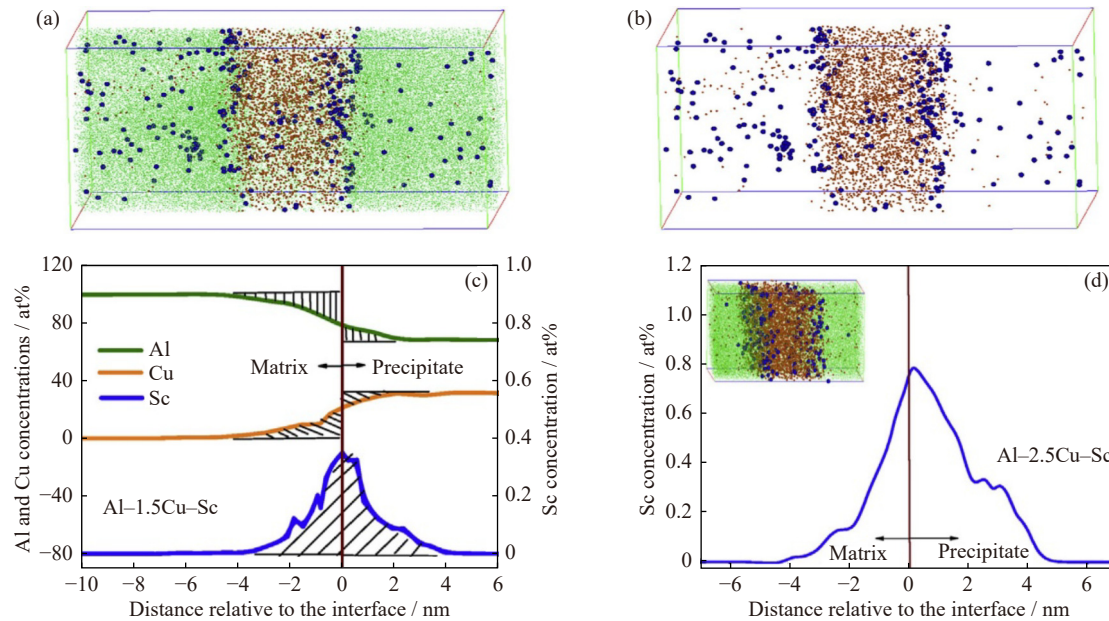


Fig. 5. APT of Al–1.5Cu–0.3Sc and Al–2.5Cu–0.3Sc alloys aged at 250°C for 8 h [94]: (a) representative APT reconstruction of a sectioned θ' precipitate in aged Al–1.5Cu–0.3Sc alloy, where Al, Cu, and Sc atoms are green, orange, and blue, respectively (dimensions: 20 nm \times 20 nm \times 40 nm); (b) corresponding APT reconstruction in (a) where only Cu and Sc atoms are presented to show the apparent distribution of Sc atoms at the interface; (c) 1D concentration profile of Al, Cu, and Sc atoms across the θ' precipitate in (a), where the solid vertical line refers to the θ' /matrix interface; (d) 1D concentration profile of Sc atoms across the θ' precipitate in aged Al–2.5Cu–0.3Sc alloy (the inset shows the corresponding APT reconstruction with dimensions of 15 nm \times 15 nm \times 30 nm). For interpretation of the references to color in this figure legend, the reader is referred to the web version of this article. Reprinted from *Acta Mater.*, Vol. 119, C. Yang, P. Zhang, D. Shao, *et al.*, The influence of Sc solute partitioning on the microalloying effect and mechanical properties of Al–Cu alloys with minor Sc addition, 68–79, Copyright 2016, with permission from Elsevier.

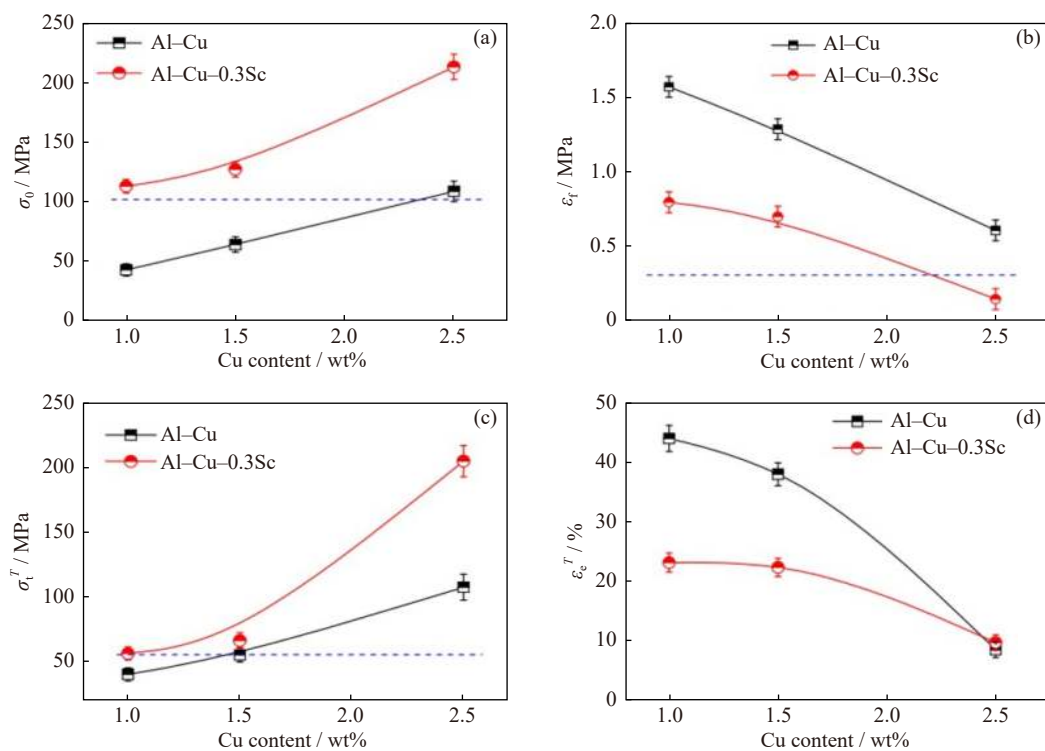


Fig. 6. Room-temperature and high-temperature (300°C) tensile results of Al–XCu and Al–XCu–0.3Sc alloy aged at 250°C for 8 h: (a) room-temperature yield strength (σ_0); (b) room-temperature fracture strain (ϵ_f); (c) tensile strength σ_t^T at 300°C; (d) elongation to failure ϵ_e^T at 300°C. Reprinted from *Acta Mater.*, Vol. 119, C. Yang, P. Zhang, D. Shao, *et al.*, The influence of Sc solute partitioning on the microalloying effect and mechanical properties of Al–Cu alloys with minor Sc addition, 68–79, Copyright 2016, with permission from Elsevier.

already formed Sc-based precipitates at 300°C [61], both inhibiting Sc atoms from segregating at the θ' /matrix interface. Thus, θ' precipitation was more promoted at 250°C aging, i.e., a more reduced precipitate size and larger number density than aging at the other two temperatures, stemming from the more improved interfacial Sc segregation inhibiting precipitate growth. As expected, a higher strength at 250°C aging was observed. However, the peak 250°C-aged Al–2.5Cu–0.3Sc alloy exhibited a sharply lower fracture strain than the peak 200°C- and 300°C-aged alloys. *In situ* TEM tensile measurements revealed interfacial decohesion at the precipitate ahead of the crack tip in the aged Al–2.5Cu–0.3Sc alloy [78]. Chen *et al.* [78] established a micromechanical model to consider the effects of both interfacial energy and precipitate size. On the one hand, the reduction in interfacial energy resulting from Sc segregation increased the critical interfacial stress [97], which prevented the interfacial decohesion. On the other hand, the reduced interfacial energy by interfacial Sc segregation resulted in a more uniform distribution of θ' precipitates with finer size, producing more geometrically necessary dislocations around the precipitates. The higher-density geometrically necessary dislocations gave rise to higher local stress at precipitates under applied loading [98–99]. When the local stress was greater than the critical interfacial stress, the fracture mechanism was interfacial decohesion-aided crack growth, resulting in a low ductility.

As stated above, Sc segregation at the θ' /matrix interface can improve the coarsening resistance of the precipitates upon heating. However, even after artificial 250°C aging for 8 h, the Sc segregation at the θ' /matrix interface in the Al–2.5Cu–0.3Sc alloy (abbreviated as Al–Cu–Sc AA) could only reach $\sim 0.8\text{at}\%$. Gao *et al.* [81] dexterously developed a modified precipitation protocol inspired by the retrogression and re-aging heat treatment in 7000-series Al alloys [100] and multistep/isochronal aging in Al–Sc-based alloys [62] to remarkably improve the interfacial Sc segregation to $\sim 2.4\text{at}\%$ (Fig. 7(a)) and further increase precipitate number density (twice higher) in the Al–2.5Cu–0.3Sc alloy (abbreviated as Al–Cu–Sc RR). The modified protocol first applies a complement additional regression treatment at 450°C for 20 min to dissolve θ' precipitates and simultaneously produce a high number density of nanosized Al_3Sc precipitates and then re-

aging at 250°C for 6 h to re-precipitate θ' heterogeneously at pre-existing Al_3Sc precipitates. Meanwhile, Sc atoms are efficiently segregated to the θ' /matrix interface, reaching a remarkable level of $\sim 2.4\text{at}\%$. Fig. 7(b) shows the results of tensile creep tests, showing that the secondary stage exhibited a surprisingly long endurance (~ 350 h) in the Al–Cu–Sc RR alloy, about a 10-fold increase compared with the Al–Cu–Sc AA. The significantly improved interfacial Sc segregation can, on the one hand, reduce the interfacial energy and, on the other hand, inhibit Cu atoms from diffusing across the interface during the creep tests. Similarly, Ag atoms segregated at the Ω /matrix interface in Al–Cu–Mg–Ag alloys reduced the interfacial energy and, concomitantly, the driving force for precipitate coarsening [101]. Thus, the coarsening resistance of θ' precipitates upon heating was significantly improved, and the Al–Cu–Sc RR alloy displayed outstanding creep resistance. An innovative interfacial segregation of multiple elements, which forms a sandwich structure to reinforce the interface, has been proposed in the Al–Cu–Sc–Fe–Si alloy [102], in which Sc and Fe are each segregated at one atomic plane and thus forming back-to-back barriers to reinforce each other. This novel structure resulting from the interfacial segregation was found to suffocate coarsening of the θ' precipitates at 300°C and cause a dramatic improvement in creep resistance. Upon extended exposure at 350°C in Al–Cu–Mn–Zr [103] and Al–Cu–Mn–Zr–Ti alloys [87], Mn diffusion into the interface of θ' precipitates was faster than Zr or Ti and stabilized θ' precipitates long enough to allow Zr or Ti to additionally segregate to the interface, remarkably improving the creep resistance. The synergistic interaction of multiple segregated elements proves to be a promising approach to improve the creep resistance of Al–Cu alloys and can be extended to other series of Al alloys. The coexistence of Al_3Sc nanoprecipitates and θ' precipitates in the Al–Cu–Sc alloys by tuning the aging treatments has shown great advantages in improving the creep resistance [104–105]. On the one hand, the Sc segregation at the θ' /matrix interface prohibited the coarsening of the θ' precipitates. On the other hand, the consumption of Sc solutes at interfacial segregation prevented the coarsening of Al_3Sc nanoprecipitates at high temperatures.

In CG Al–Cu alloys, the Sc microalloying effects mainly

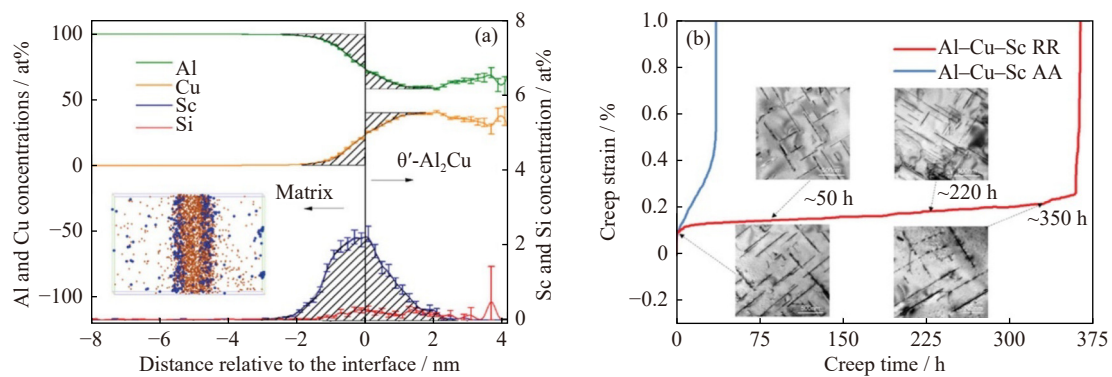


Fig. 7. (a) Representative proxigrams of Al, Cu, Sc, and Si across θ' precipitates in Al–Cu–Sc RR alloy; (b) tensile creep curves of Al–Cu–Sc RR alloy at 300°C and 30 MPa [81].

depend on (i) the formation of Cu/Sc/vacancy complexes that act as preferential nucleation sites for θ' precipitates and (ii) the Sc segregation at the θ' /matrix interface that reduces the interfacial energy and inhibits precipitate growth. It is confirmed that the outstanding Sc microalloying effects in CG Al–Cu alloys are efficient at artificially controlling the precipitation and improving the mechanical properties at room and high temperatures, especially the creep resistance.

4. Fine/ultrafine-grained Al–Cu alloys with Sc microalloying

During the past two decades, ECAP has been widely adopted to produce fine-grained (with a grain size of one to several micrometers, abbreviated as FG) and ultrafine-grained (with a grain size of hundreds of nanometers to one micrometer, abbreviated as UFG) Al alloys [106–107]. Grain refining mechanisms are based on the concept of dynamic recrystallization, i.e., the initial dislocation accumulation in the form of a dislocation cell transforms gradually to the final fine grain structure with deformation [108–109]. The applied high strain can introduce a high density of defects (such as dislocations, vacancies, and grain boundaries), which can greatly accelerate atom diffusion and increase the precipitation kinetics by several orders of magnitude, resulting in preferentially intergranular precipitation even during storage in ambient conditions [54], which are detrimental to strength, ductility, and corrosion resistance [110–112]. In the ECAP-processed Al–Cu alloy, low-temperature aging [113–114] or storage in ambient conditions [54] can cause an extensive intergranular θ precipitation, skipping the metastable equilibrium θ' precipitates. During subsequent artificial aging in the ECAP-processed 7075 alloy, the precipitation kinetics was significantly accelerated compared with that in the CG alloy and the precipitation sequence (i.e., solid solution \rightarrow GP zone \rightarrow η' \rightarrow η) did not change [12]. Sha *et al.* [57] examined the dynamic aging precipitation behaviors in the ECAP-processed Al–Zn–Mg–Cu alloy at 200°C and observed that ECAP changed the orientation of η precipitates into equiaxial growth. Similarly, during subsequent artificial aging in the ECAP-processed Al–Mg–Si alloy, the precipitation sequence did not change and the precipitation kinetics was greatly accelerated along with the alteration in morphology of the precipitate [115]. The extensively adopted microalloying method in CG Al alloys offer opportunities to alter such disadvantage precipitation behaviors in Al alloys processed by SPD.

Extensive intergranular equilibrium θ precipitation in SPD-processed Al–Cu alloys at low temperatures or even ambient conditions is a long-standing problem to practical application. Jiang *et al.* [53,58,79] obtained FG/UFG Al–2.5Cu alloys and FG/UFG Al–2.5Cu–0.3Sc alloys by ECAP through controlling pass numbers. After 125°C aging for 20 h, both intergranular θ precipitation and intragranular θ' precipitation can be detected in the FG Al–2.5Cu alloy (Fig. 8(a)). Fig. 8(b) shows that minor Sc addition in the FG

Al–2.5Cu–0.3Sc alloy suppressed partial intergranular θ precipitation, where only intragranular θ' precipitation was present. In the aged UFG Al–2.5Cu alloy (Fig. 8(c)), only intergranular θ precipitation was observed. Similarly, minor Sc addition resulted in complete intragranular θ' precipitation in the UFG Al–2.5Cu–0.3Sc alloy (Fig. 8(d)), which has a larger average size and a lower number density of θ' precipitates compared with the aged FG Al–2.5Cu–0.3Sc (Fig. 8(b)). The UFG Al–2.5Cu–0.3Sc alloy has higher dislocation density and vacancy concentration ($10.98 \times 10^{14} \text{ m}^{-2}$ and $(3.0 \times 10^{-3})\text{at}\%$, respectively) than the FG Al–2.5Cu–0.3Sc alloy ($7.29 \times 10^{14} \text{ m}^{-2}$ and $(2.3 \times 10^{-3})\text{at}\%$, respectively). The higher dislocation density and vacancy concentration resulted in larger growth kinetics of θ' precipitates in the UFG Al–2.5Cu–0.3Sc alloy. The strengthening effects of shear-resistant plate-like θ' precipitates $\sigma_{\text{P}}^{\text{Intra}}$ can be calculated using Eqs. (1) and (2) [91],

$$\lambda_{\text{ave}} = \sqrt{\frac{\sqrt{3}}{2} \frac{1}{\sqrt{\sin\theta \cdot N \cdot L}} - \frac{\pi L}{8} - \frac{\sqrt{3}}{2} \frac{h}{\sin\theta}} \quad (1)$$

$$\sigma_{\text{P}}^{\text{Intra}} = \frac{M\mu b}{2\pi\sqrt{1-\nu}} \frac{1}{\lambda_{\text{ave}}} \ln\left(\frac{r_o}{r_i}\right) \quad (2)$$

where λ_{ave} refers to the average spacing between plate tips, N refers to the number of precipitates per unit volume, L refers to their length, h refers to their thickness, θ refers to the dihedral angle between the plate and the $\{111\}_{\alpha}$ slip plane (for the $\{001\}_{\alpha}$ precipitate plates, $\theta = 54.74^\circ$), M refers to the Taylor factor (~ 3.1), μ is the shear modulus of matrix, ν represents Poisson's ratio (~ 0.33), b indicates the Burgers vec-

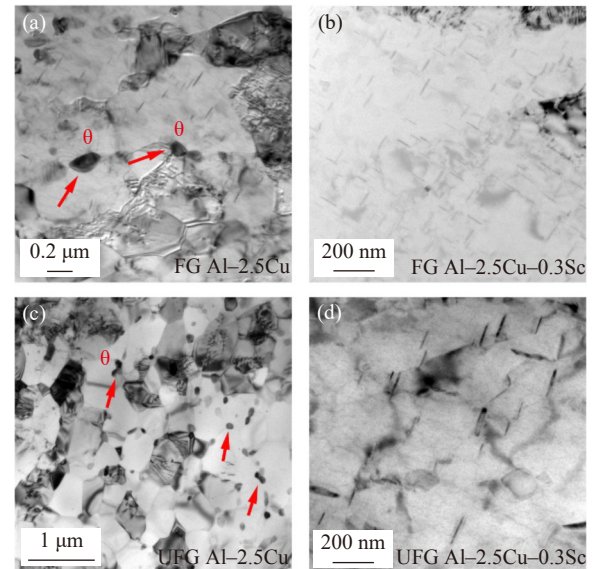


Fig. 8. Typical bright-field TEM images showing the precipitation behaviors in FG/UFG Al–2.5Cu and Al–2.5Cu–0.3Sc alloys at 125°C aging for 20 h [80]: (a) FG Al–2.5Cu; (b) FG Al–2.5Cu–0.3Sc; (c) UFG Al–2.5Cu; (d) UFG Al–2.5Cu–0.3Sc. Reprinted from *Mater. Sci. Eng. A*, Vol. 721, S.H. Wu, P. Zhang, D. Shao, *et al.*, Grain size-dependent Sc microalloying effect on the yield strength–pitting corrosion correlation in Al–Cu alloys, 200–214, Copyright 2018, with permission from Elsevier.

tor (0.286 nm), and r_i and r_o refer to the inner and outer cutoff radius of the dislocation (using $r_i = |b|$ (0.286 nm) and $r_o = 3.5h^3$), respectively. Table 4 in reference [53] revealed that the strengthening contributions from intragranular θ' precipitates in the peak-aged FG and UFG Al–2.5Cu–0.3Sc alloys were about 125 and 145 MPa, respectively, although the average size of the θ' precipitates was larger and the number density was lower in the peak-aged UFG Al–2.5Cu–0.3Sc alloy.

Therefore, a smaller grain size results in a more significant Sc microalloying effect. The as-deformed UFG Al–2.5Cu–0.3Sc had a vacancy concentration of $\sim(3.0 \times 10^{-3})\text{at}\%$ compared with the as-deformed UFG Al–2.5Cu alloy ($\sim(1.6 \times 10^{-6})\text{at}\%$) as measured by positron annihilation lifetime spectroscopy. In addition, APT analysis confirmed that a significant number density of clusters was present in the as-deformed UFG Al–2.5Cu–0.3Sc alloy, while there was no apparent cluster in the as-deformed UFG Al–2.5Cu alloy. Thus, the length-scale dependent Sc microalloying effects on the precipitation behaviors in ECAP-processed Al–Cu alloys can be understood as follows: (i) a several orders of magnitude lower diffusion coefficient of Sc than Cu [78] guarantees that the majority of Sc atoms remained within the matrix even at high temperatures (e.g., at 125°C, the diffusion coefficient of Sc in the Al matrix (D_{Sc}) is about $5.67 \times 10^{-26} \text{ m}^2 \cdot \text{s}^{-1}$ and the diffusion coefficient of Cu (D_{Cu}) has a several orders higher value of about $1.13 \times 10^{-22} \text{ m}^2 \cdot \text{s}^{-1}$ [61]; (ii) the Cu/Sc/vacancy complex clusters of strong binding [116–117] within the grain interior act as preferential nucleation sites for intragranular θ' precipitates and inhibit both Cu atoms and vacancies from diffusing toward grain boundaries. Fig. 9 depicts the tensile test results, revealing that the poor tensile performance in the aged UFG Al–2.5Cu alloy (tensile strength ~ 300 MPa, fracture strain $\sim 4\%$) was much better improved in the aged UFG Al–2.5Cu–0.3Sc alloy (tensile strength ~ 460 MPa, fracture strain $\sim 15\%$), strongly showcasing that the length-scale dependent Sc mi-

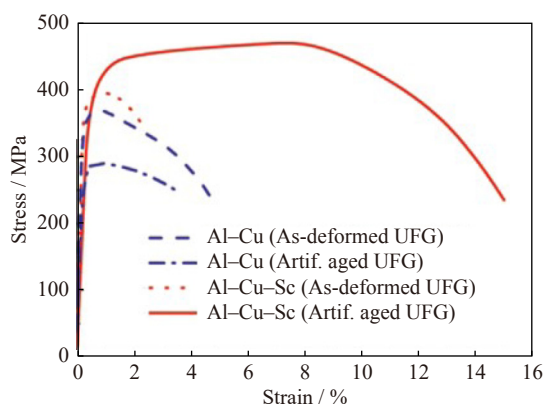


Fig. 9. Typical tensile engineering stress–strain curves of the as-deformed and aged UFG Al–2.5Cu/Al–2.5Cu–0.3Sc alloys [53]. Reprinted from *Mater. Sci. Eng. A*, Vol. 637, L. Jiang, J.K. Li, G. Liu, *et al.*, Length-scale dependent microalloying effects on precipitation behaviors and mechanical properties of Al–Cu alloys with minor Sc addition, 139–154, Copyright 2015, with permission from Elsevier.

croalloying effect can efficiently change precipitation behaviors (e.g., the size, chemistry, and spatial distribution) and improve mechanical properties.

Similarly, the Sc segregation at the θ' /matrix interface also exhibited a grain size dependence in addition to the dependence on Cu content and aging temperature in CG Al–Cu alloys. According to a study by Wu *et al.* [80], with reducing grain size, the interfacial Sc segregation increased from $\sim 0.8\text{at}\%$ in the peak-aged CG Al–2.5Cu–0.3Sc alloy to $\sim 3.0\text{at}\%$ in the peak-aged FG Al–2.5Cu–0.3Sc alloy and stepwise further to $\sim 12.0\text{at}\%$ in the peak-aged UFG Al–2.5Cu–0.3Sc alloy. On the one hand, interfacial Sc segregation can significantly change the precipitation behaviors (i.e., precipitate size and spatial distribution); on the other hand, the concomitantly modified interfacial structure also influences corrosion resistance [118]. The reduced interfacial energy by Sc segregation can effectively inhibit the interfacial chemical activity and also narrow the electrochemical incompatibility between θ' precipitates and Al matrix, which is beneficial for corrosion resistance. Meanwhile, the deformation-introduced high-density dislocations are harmful to corrosion resistance [110–111]. In the peak-aged CG and UFG Al–2.5Cu alloys, pitting resistance was improved by minor Sc addition, in which pitting potential is more positive (Fig. 10(a)) and metastable pitting events are fewer (CG Al–2.5Cu–0.3Sc) or almost unchanged (UFG Al–2.5Cu–0.3Sc) (Fig. 10(b)). In the peak-aged CG Al–2.5Cu–0.3Sc alloy, the interfacial Sc segregation ameliorated the pitting resistance. Moreover, the peak-aged UFG Al–2.5Cu–0.3Sc alloy showed that the positive effect of interfacial Sc segregation on pitting resistance dominated over the negative effect of tangled dislocations. However, the pitting resistance of the peak-aged FG Al–2.5Cu alloy seldom change after minor Sc addition, which was ascribed to the negative dominance of dislocations over the interfacial Sc segregation in turn. Therefore, the inverse correlation between strength and pitting resistance generally existing in Al alloys [50, 119–120] was broken in the peak-aged CG Al–2.5Cu–0.3Sc and UFG Al–2.5Cu–0.3Sc. The length-scale dependent Sc microalloying effect in the UFG Al–2.5Cu–0.3Sc alloy was confirmed to improve both the strength/ductility synergy and pitting resistance.

Heterogeneous grain structures can improve both strength and ductility, which is related to the introduced excessively large number of geometrically necessary dislocations to accommodate the large strain gradient during tensile deformation, resulting in additional strain hardening [121–123]. ECAP at cryogenic temperature introduced hierarchical microstructures of multimodal grains, low-angle grain boundaries, and intergranular/intragranular precipitates tuned by artificial aging in the Al–2.5Cu alloy [82], demonstrating a promoted strength–ductility synergy. A minor 0.3wt% Sc addition was effective in improving intragranular precipitation and completely suppressing intergranular precipitation, similar to room-temperature ECAP, thus further enhancing the strength–ductility synergy.

Fig. 11 illustrates the modified Al–Cu binary phase dia-

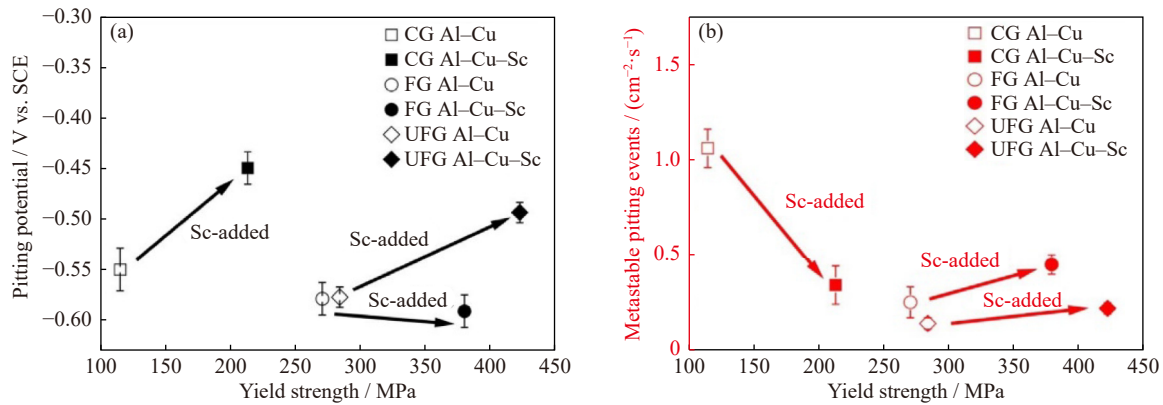


Fig. 10. (a) Correlations between pitting potential and yield strength and (b) metastable pitting events and yield strength in the peak-aged (CG, FG, UFG) Al–Cu and Al–Cu–Sc alloys [80]. Reprinted from *Mater. Sci. Eng. A*, Vol. 721, S.H. Wu, P. Zhang, D. Shao, *et al.*, Grain size-dependent Sc microalloying effect on the yield strength–pitting corrosion correlation in Al–Cu alloys, 200–214, Copyright 2018, with permission from Elsevier.

gram, showing the length-scale dependent Sc microalloying effects on the precipitation behaviors in FG/UFG Al–Cu alloys. Because a large quantity of nonequilibrium defects was present in the FG/UFG Al–Cu alloys, the significantly accelerated atomic diffusion resulted in intergranular θ precipitation at ambient temperature, much lower than the required temperature ($\sim 420^\circ\text{C}$). Minor Sc addition in FG/UFG Al–2.5Cu–0.3Sc alloys promoted intragranular θ' precipitation at 125°C aging, also lower than the thermodynamically required temperature ($\sim 200^\circ\text{C}$). In conclusion, the equilibrium phase diagram needs further investigations for application in FG/UFG alloys or other nonequilibrium Al alloys.

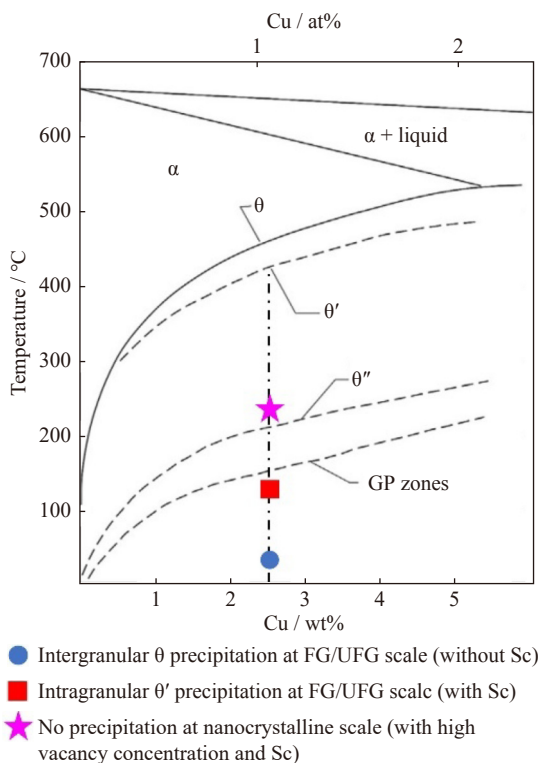


Fig. 11. Modified Al–Cu binary phase diagram at the Al-rich side. Adapted from *Physical Metallurgy*, J.F. Nie, *Physical metallurgy of light alloys*, 2009–2156, Copyright 2014, with permission from Elsevier.

5. Nanocrystalline Al–Cu alloys with Sc microalloying

In ECAP, limited shear strain (~ 1 after one pass) [124] can be introduced during deformation, confining the obtainable grain scale minimum to UFG. HPT has been extensively employed in the production of nanocrystalline (grain size of several to 100 nm) Al alloys [43,47–48] because the introduced shear strain by HPT can reach several hundred [125–126]. Room-temperature superplasticity was observed for room-temperature HPT-processed nanocrystalline Al–Zn alloys [127–128], which was realized by grain boundary sliding and grain rotation with the help of continuous Zn diffusion. Supersaturated Al–Zn alloys were produced by ultra-HPT with a shear strain of up to 40000 [129]. During subsequent artificial aging, coherent metastable Al_3Zr precipitates were found within the grain interiors, confirming an outstanding hardness of up to HV 148. Encouragingly, SPD at liquid nitrogen/cryogenic temperatures presents the ability to efficiently improve the strength–ductility synergy, which originates from the suppressed dynamic recovery and dynamic precipitation during SPD deformation [130–132]. HPT in liquid nitrogen (with a high rotating speed) was applied by Lu's group to obtain a novel Schwarz crystal structure of extremely small grain size of ~ 10 nm, which imparted high strength and thermal stability to metallic materials [43–44,131]. The original work [39] revealed that the coupling influences of Sc microalloying and cryogenic temperature on HPT-generated nanocrystalline Al–Cu alloys show a new phenomenon, which is different from what is expected.

The work by Wu *et al.* [39] employed HPT in liquid nitrogen to produce nanocrystalline Al–2.5Cu–0.3Sc alloy (denoted as AlCuSc-C), where equiaxial nanosized grains (with ~ 100 nm average grain size) and no apparent element segregation were observed (Fig. 12(a) and (b)). In addition, they performed room-temperature HPT to fabricate nanocrystalline Al–2.5Cu and Al–2.5Cu–0.3Sc alloys (abbreviated as AlCu-R and AlCuSc-R, respectively) and liquid nitrogen HPT to prepare nanocrystalline Al–2.5Cu alloy (abbreviated

as AlCu-C) for comparison. By utilizing the positron standard trapping models and diffusion trapping models [133–134] to analyze the positron annihilation lifetime spectroscopy results, as quantitatively presented in Fig. 12(c), it is interesting to find that the vacancy concentration in the AlCuSc-C alloy reached $\sim 0.22\text{at}\%$ (Fig. 12(c)), one to two orders of magnitude higher than those in other ECAP- and HPT-processed Al alloys, including the AlCu-R, AlCu-C, and AlCuSc-R alloys. During HPT processing, collisions from moving dislocations produce vacancies. Sauvage *et al.* [135] performed room-temperature HPT on Al-5.8wt%Mg alloy and found that the generating rate of vacancies could reach $\sim 10^{-5} \text{ s}^{-1}$. However, vacancies are prone to migrate to

the deformation-introduced defects (e.g., nonequilibrium grain boundaries and dislocations) to annihilate [136], leading to the typical vacancy concentration of only $\sim 10^{-5}$ after HPT processing for 600 s (only 1/600 of the produced vacancies) in Al alloys. Compared with liquid nitrogen HPT for 600 s, the AlCuSc-C alloy had a vacancy concentration of $\sim 0.22\text{at}\%$, about a third of the theoretical maximum vacancy concentration. In addition, a vast number density of (Cu, Sc, vacancy)-rich atomic complexes (with an average size of $\sim 1\text{--}2 \text{ nm}$ and a volumetric number density of $\sim 2.0 \times 10^{24} \text{ m}^{-3}$) were present in the matrix (Fig. 12(d)–(f)). Fig. 12(f) displays the inverse fast Fourier transform (FFT) image of Fig. 12(e).

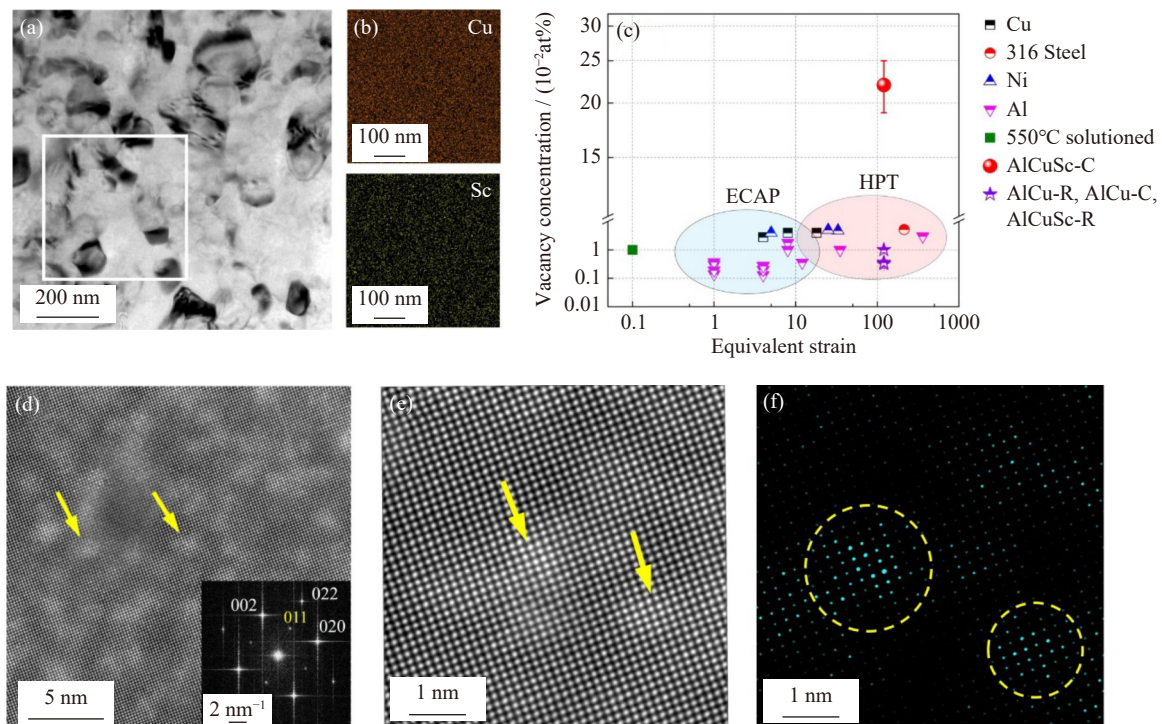


Fig. 12. (a) Representative bright-field TEM image of the AlCuSc-C alloy showing the uniform nanograins; (b) corresponding Cu and Sc elemental energy dispersive spectrometer (EDS) mapping in the rectangular area in (a); (c) comparison of vacancy concentrations between the AlCuSc-C alloy and other small-grained alloys; (d) atomic-resolution high-angle annular dark-field (HAADF)-scanning transmission electron microscope (STEM) image showing high-density atomic complexes in the AlCuSc-C alloy viewed along the $\langle 100 \rangle_{\text{Al}}$ where the inset is the corresponding FFT pattern; (e) typical atomic complexes in the AlCuSc-C alloy by HAADF-STEM along the $\langle 100 \rangle_{\text{Al}}$; (f) corresponding inverse FFT image in (e) showing the atom complexes enriched with Cu and Sc [39].

The positron annihilation lifetime spectroscopy results revealed that the measured lifetime in the AlCuSc-C alloy originated from positron annihilation in bulk monovacancies and bulk divacancies (Fig. 1(f) in reference [39]). Density functional theory (DFT) calculation results shown in Fig. 13(a) revealed that the Cu–Sc–2 vacancy complex had a higher binding energy ($\sim 0.35 \text{ eV}$) than the Cu–Sc–vacancy complex. It was reasonably inferred that during cryogenic HPT, the majority of produced vacancies were stabilized in Cu–Sc–2 vacancy complexes, considering a concentration ratio of vacancy/Sc of ~ 1.4 . Cu–Sc–2 vacancy complexes absorbed more Cu and Sc atoms aside from vacancies, generating larger-sized (Cu, Sc, vacancy)-rich atomic complexes, which also showed high thermal stability. Fig. 13(b) depicts

the differential scanning calorimetry (DSC) results, indicating that the precipitation temperature was delayed until 200°C . In fact, even after aging at 225°C for 50 h, where apparent recrystallization occurred, the AlCuSc-C alloy had no obvious precipitation (Fig. 3(c) in reference [39]). In Fig. 13(c), in general, the thermal instability temperature (where extensive precipitation of stable precipitates occurred during aging for 50 h) rapidly decreased with deformation strain exerted on the alloys. The balancing dilemma was broken in the AlCuSc-C alloy. With the higher binding energy and much lower diffusivity of Sc atoms compared with Cu atoms, vacancies in (Cu, Sc, vacancy)-rich atomic complexes prevented Cu and vacancies from being effectively involved in the precipitation of both intragranular θ' and intergranular θ

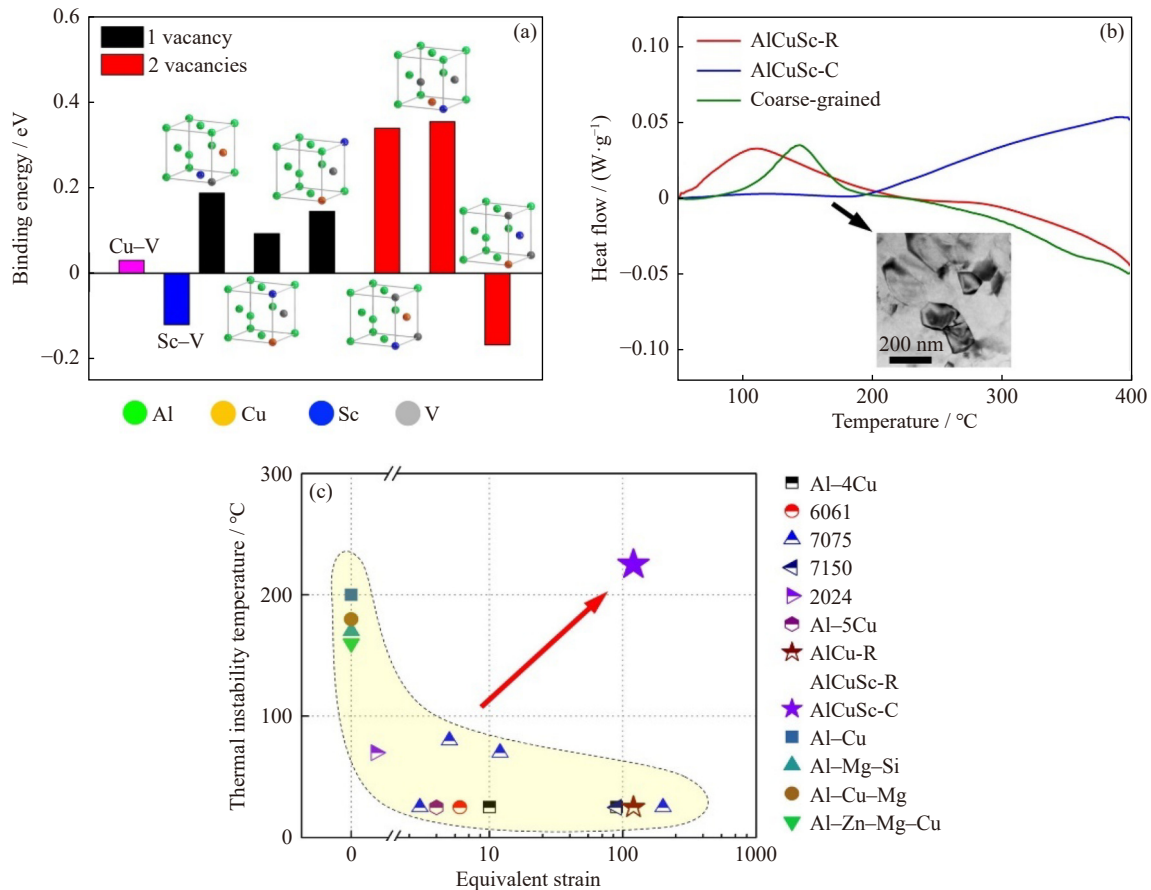


Fig. 13. (a) DFT-calculated binding energies of the Cu–Sc– X ($X = 1, 2$) vacancy complex (V denotes vacancy); (b) DSC heating curves of the AlCuSc-R, AlCuSc-C alloys, and CG Al–Cu–Sc alloy, where the inset is a typical bright-field TEM image of the AlCuSc-C alloy aged at 175°C for 50 h; (c) statistical thermal instability temperatures of some typical cast Al alloys and AlCuSc-C alloy [39].

phases in the AlCuSc-C alloy. Comparison with 125°C aging or even ambient storage showed that large quantities of intragranular or intergranular θ precipitation were induced in the AlCu-R, AlCu-C, and AlCuSc-R alloys [39]. Compared with aged FG/UFG Al–2.5Cu–0.3Sc alloys, no intragranular θ' precipitates were observed in the aged AlCuSc-R alloy, which may be associated with the much smaller grain size, higher dislocation density, and vacancy density in the AlCuSc-R alloy, leading to a significantly larger precipitation kinetics. The above factors promoted intragranular θ precipitation and skipped the metastable equilibrium θ' phase.

Actually, as confirmed in Fig. 11, aging at 225°C can lead to the formation of the θ' phase. The length-scale dependent Sc microalloying effect in nanocrystalline Al–Cu–Sc alloys coupled with the retained high-density vacancies result in no obvious precipitation when aging at 225°C.

Fig. 14(a) plots the engineering stress–strain curves, demonstrating that the AlCuSc-C alloy had a much better strength–ductility synergy than the AlCuSc-R alloy and CG Al–2.5Cu and Al–2.5Cu–0.3Sc alloys. Micropillar compression tests (micropillars of the same diameter $\sim 1 \mu\text{m}$) [137] performed on the AlCuSc-C alloy (Fig. 14(b)) showed that at the same strain rate of $2 \times 10^{-4} \text{ s}^{-1}$, the AlCuSc-C alloy exhibited a stronger strain hardening ability than the AlCuSc-R alloy, with the initial strain hardening rate being higher and β

(characteristic of dynamic recovery) being lower in the former alloy (inset in Fig. 14(b)). Increasing the strain rate to $2 \times 10^{-2} \text{ s}^{-1}$, the AlCuSc-C alloys displayed a reduction in flow stress, characteristic of a negative strain rate sensitivity (SRS). Negative SRS is often reported in solution strengthening Al–Mg alloys with high Mg content, which can be explained in terms of dynamic strain aging (DSA) [138–139]. The high-density (Cu, Sc, vacancy)-rich atomic complexes in the grain interior were strong obstacles to the moving dislocations, effectively increasing the opportunity for the dislocations to interact with each other. The improved moving resistance of the dislocations could greatly promote the dislocation storage ability inside the nanosized grains, thus remarkably improving the strain hardening ability [140]. As a consequence, the AlCuSc-C alloys had a remarkable strength–ductility synergy (tensile strength $\sim 570 \text{ MPa}$ and uniform ductility $\sim 8.5\%$). The negative SRS in the AlCuSc-C alloy could be rationalized based on the Kubin and Estrin models [138–139]. The waiting time of pinned dislocations spent at localized obstacles (t_w) is normally longer than the time spent by dislocations to move freely between obstacles [141]. With a sufficient supply of solute atoms pinning dislocations, the characteristic time for solute atoms diffusing toward the temporarily arrested dislocations at localized obstacles is t_d . The DSA occurs provided that t_w and t_d have

the same order of magnitude, i.e., the t_w of arrested dislocations allows the solute atoms to diffuse toward the dislocations and then efficiently pin them [142]. Due to the small size of (Cu, Sc, vacancy)-rich atomic complexes ($\sim 1\text{--}2$ nm), the atomic complexes could be sheared by the moving dislocations. The released high-density vacancies could accelerate the diffusion of Cu and Sc atoms toward the temporarily arrested dislocations. In addition, due to the strong binding energy of the (Cu, Sc, vacancy)-rich atomic complexes, new

atomic complexes could form rapidly at the arrested dislocations, exerting an additional stress on the slipping dislocations. However, applying a much higher strain rate of $2 \times 10^{-2} \text{ s}^{-1}$, there was insufficient time for the released vacancies to promote the discrete Cu and Sc atoms diffusing toward the arrested dislocations, i.e., t_w is smaller than t_d . As a result, the pinning effects of (Cu, Sc, vacancy)-rich atomic complexes on the moving dislocations were reduced, thus reducing the strain hardening ability of the AlCuSc-C alloy.

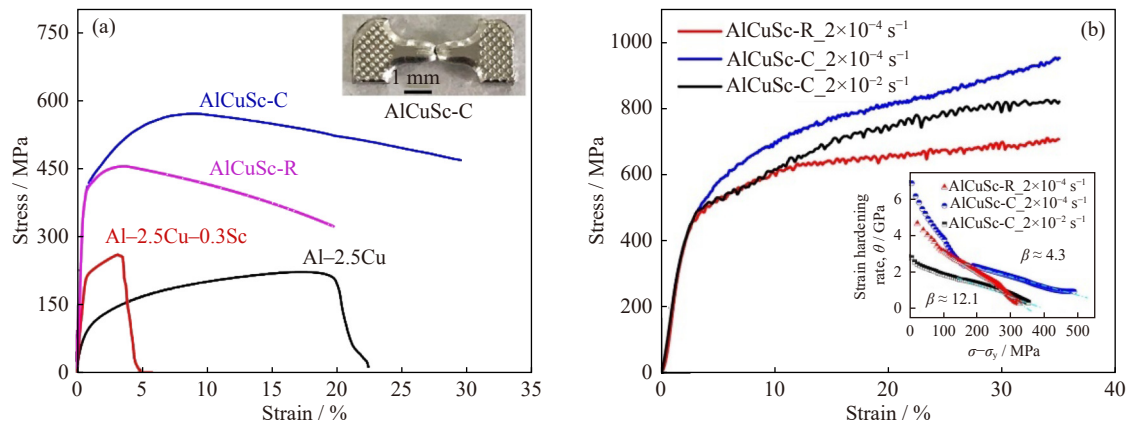


Fig. 14. (a) Typical tensile stress–strain curves of the peak-aged CG Al-2.5Cu, Al-2.5Cu-0.3Sc, AlCuSc-R, and AlCuSc-C alloys, where the inset is the fractured tensile specimen of the AlCuSc-C alloy; (b) micropillar compressing results with a diameter of $1 \mu\text{m}$ in the AlCuSc-R and AlCuSc-C alloys at different strain rates, where the inset is the corresponding Kocks–Mecking plots [39]. σ is the flow stress and σ_y is the yield strength.

The combination of liquid nitrogen HPT and Sc microalloying effects introduced both high-density vacancies and large quantities of (Cu, Sc, vacancies)-rich atomic complexes in the nanocrystalline Al-Cu-Sc alloy. Such ordered atomic complexes are similar to the extensively studied chemical short-range order in high-entropy alloys [140,143] and the strengthening and irradiation-resistant B2 phase (Ni(Al,Fe) precipitates) in the ultrastrong steel [144–145].

6. Conclusions and perspectives

Sc, as an extensively applied microalloying element, has been shown to significantly affect the microstructures and properties of Al alloys. Unlike only examining the microalloying effects in CG Al alloys, systematic studies on the length-scale dependent Sc microalloying effects in Al-Cu alloys disclosed in-depth the interactions between the microalloying element Sc and the alloying element Cu and structural defects (e.g., vacancies), which can be applied to artificially control the precipitation behaviors across the wide range of grain sizes, thus changing the mechanical properties, corrosion properties, and thermal stabilities.

(1) In CG Al-Cu alloys, minor Sc addition arrested quenching vacancies to seize Cu atoms, being arranged in the Cu/Sc/vacancies complexes acting as heterogeneous nuclei for θ' precipitation. The Cu content affected significantly the dissolved Sc content in the matrix, i.e., a higher Cu content resulting in a larger Sc solubility. Thus, Sc segregation at the θ' /matrix interface exhibited a positive relation with the Cu

content, which effectively inhibited precipitate growth and thus promoted the precipitation. In addition, interfacial Sc segregation shows a non-monotonic aging temperature dependence, with the strongest segregation when aging at 250°C . A modified heat treatment protocol (additional regression at high temperature and re-aging) designed to remarkably increase the interfacial Sc segregation to a high level proved to be efficient at improving the creep resistance.

(2) The FG/UFG Al-Cu alloys inevitably showed low-temperature or even ambient catastrophic intergranular θ precipitation. Due to the much lower diffusivity of Sc atoms, the formation of Cu/Sc/vacancies complexes in the FG/UFG Al-Cu-Sc alloys refrained the Cu and vacancies from escaping toward the grain boundaries, which promoted the desired intragranular θ' precipitation. The most significant Sc microalloying effect was found in the UFG Al-Cu-Sc alloy, where the interfacial Sc segregation could reach $\sim 12.0\text{at}\%$. The high-density intragranular θ' precipitates and high-level interfacial Sc segregation endowed the UFG Al-Cu-Sc alloy with an excellent combination of strength–ductility synergy and pitting resistance.

(3) Applying high strain by liquid nitrogen HPT to form nanocrystalline Al-Cu-Sc alloys, the formation of a high-density (Cu, Sc, vacancy)-rich atomic complexes with high thermal stability, induced by the high retained vacancy concentration, suppressed the supersaturated solid solution from decomposing until 225°C . The homogeneously distributed (Cu, Sc, vacancy)-rich atomic complexes obstructed the moving dislocations and significantly enhanced the strain

hardening capacity. The intractable low-temperature precipitation and insufficient ductility in heat-treatable nanocrystalline Al–Cu alloys can be overcome by the length-scale dependent Sc microalloying effects assisted by the high-density vacancies.

Acknowledgements

This work was supported by the National Natural Science Foundation of China (Nos. 52201135, 52271115, U23A6013, 92360301, and U2330203), the 111 Project of China (No. BP2018008), and the Shaanxi Province Innovation Team Project, China (No. 2024RS-CXTD-58). This work was also supported by the International Joint Laboratory for Micro/Nano Manufacturing and Measurement Technologies and by the open research fund of Suzhou Laboratory.

Conflict of Interest

Gang Liu is an editorial board member for this journal and was not involved in the editorial review or the decision to publish this article. The authors declare that they have no known competing financial interests or personal relationships that could have appeared to influence the work reported in this paper.

References

- [1] J.W. Martin, *Precipitation Hardening*, 2nd ed., Butterworth-Heinemann, Woburn, MA, 1998.
- [2] A. Deschamps and C.R. Hutchinson, Precipitation kinetics in metallic alloys: Experiments and modeling, *Acta Mater.*, 220(2021), art. No. 117338.
- [3] D.A. Porter and K.E. Easterling, *Phase Transformations in Metals and Alloys*, 2nd ed., CRC Press, Boca Raton, 1992.
- [4] L. Bourgeois, Y. Zhang, Z.Z. Zhang, Y.Q. Chen, and N.V. Medhekar, Transforming solid-state precipitates via excess vacancies, *Nat. Commun.*, 11(2020), No. 1, art. No. 1248.
- [5] Y.Q. Chen, Z.Z. Zhang, Z. Chen, et al., The enhanced theta-prime (θ') precipitation in an Al–Cu alloy with trace Au additions, *Acta Mater.*, 125(2017), p. 340.
- [6] K.C. Russell, Nucleation in solids: The induction and steady state effects, *Adv. Colloid Interface Sci.*, 13(1980), No. 3-4, p. 205.
- [7] C. Zener, Theory of growth of spherical precipitates from solid solution, *J. Appl. Phys.*, 20(1949), No. 10, p. 950.
- [8] J.D. Boyd and R.B. Nicholson, A calorimetric determination of precipitate interfacial energies in two Al–Cu alloys, *Acta Metall.*, 19(1971), No. 10, p. 1101.
- [9] G. Liu, G.J. Zhang, X.D. Ding, J. Sun, and K.H. Chen, Modeling the strengthening response to aging process of heat-treatable aluminum alloys containing plate/disc- or rod/needle-shaped precipitates, *Mater. Sci. Eng. A*, 344(2003), No. 1-2, p. 113.
- [10] G. Liu, J. Sun, C.W. Nan, and K.H. Chen, Experiment and multiscale modeling of the coupled influence of constituents and precipitates on the ductile fracture of heat-treatable aluminum alloys, *Acta Mater.*, 53(2005), No. 12, p. 3459.
- [11] Ø. Grong and H.R. Shercliff, Microstructural modelling in metals processing, *Prog. Mater. Sci.*, 47(2002), No. 2, p. 163.
- [12] Y.H. Zhao, X.Z. Liao, Z. Jin, R.Z. Valiev, and Y.T. Zhu, Microstructures and mechanical properties of ultrafine grained 7075 Al alloy processed by ECAP and their evolutions during annealing, *Acta Mater.*, 52(2004), No. 15, p. 4589.
- [13] Y.X. Geng, H. Tang, J.H. Xu, et al., Influence of process parameters and aging treatment on the microstructure and mechanical properties of AlSi8Mg3 alloy fabricated by selective laser melting, *Int. J. Miner. Metall. Mater.*, 29(2022), No. 9, p. 1770.
- [14] V. Radmilovic, C. Ophus, E.A. Marquis, et al., Highly monodisperse core-shell particles created by solid-state reactions, *Nat. Mater.*, 10(2011), No. 9, p. 710.
- [15] S.P. Yuan, G. Liu, R.H. Wang, et al., Coupling effect of multiple precipitates on the ductile fracture of aged Al–Mg–Si alloys, *Scripta Mater.*, 57(2007), No. 9, p. 865.
- [16] G. Liu, G. Zhang, R. Wang, W. Hu, J. Sun, and K. Chen, Heat treatment-modulated coupling effect of multi-scale second-phase particles on the ductile fracture of aged aluminum alloys, *Acta Mater.*, 55(2007), No. 1, p. 273.
- [17] M.J. Starink and S.C. Wang, A model for the yield strength of overaged Al–Zn–Mg–Cu alloys, *Acta Mater.*, 51(2003), No. 17, p. 5131.
- [18] O.R. Myhr, Ø. Grong, and S.J. Andersen, Modelling of the age hardening behaviour of Al–Mg–Si alloys, *Acta Mater.*, 49(2001), No. 1, p. 65.
- [19] S.P. Ringer and K. Hono, Microstructural evolution and age hardening in aluminium alloys: Atom probe field-ion microscopy and transmission electron microscopy studies, *Mater. Charact.*, 44(2000), No. 1-2, p. 101.
- [20] L.Z. He, Y.H. Cao, Y.Z. Zhou, and J.Z. Cui, Effects of Ag addition on the microstructures and properties of Al–Mg–Si–Cu alloys, *Int. J. Miner. Metall. Mater.*, 25(2018), No. 1, p. 62.
- [21] J.Y. Zhang, Y.H. Gao, C. Yang, et al., Microalloying Al alloys with Sc: A review, *Rare Met.*, 39(2020), No. 6, p. 636.
- [22] K. Ganjehfard, R. Taghiabadi, M.T. Noghani, and M.H. Ghoncheh, Tensile properties and hot tearing susceptibility of cast Al–Cu alloys containing excess Fe and Si, *Int. J. Miner. Metall. Mater.*, 28(2021), No. 4, p. 718.
- [23] H.K. Hardy, The ageing characteristics of ternary aluminium–copper alloys with cadmium, indium, or tin, *J. Inst. Met.*, 80(1952), p. 483.
- [24] L. Bourgeois, C. Dwyer, M. Weyland, J.F. Nie, and B.C. Muddle, The magic thicknesses of θ' precipitates in Sn-microalloyed Al–Cu, *Acta Mater.*, 60(2012), No. 2, p. 633.
- [25] L. Bourgeois, J.F. Nie, and B.C. Muddle, Assisted nucleation of θ' phase in Al–Cu–Sn: The modified crystallography of tin precipitates, *Philos. Mag.*, 85(2005), No. 29, p. 3487.
- [26] T. Homma, M.P. Moody, D.W. Saxey, and S.P. Ringer, Effect of Sn addition in preprecipitation stage in Al–Cu alloys: A correlative transmission electron microscopy and atom probe tomography study, *Metall. Mater. Trans. A*, 43(2012), No. 7, p. 2192.
- [27] D. Mitlin, J.W. Morris, V. Radmilovic, and U. Dahmen, Precipitation and aging in Al–Si–Ge–Cu, *Metall. Mater. Trans. A*, 32(2001), No. 1, p. 197.
- [28] T. Sato, S. Hirose, K. Hirose, and T. Maeguchi, Roles of microalloying elements on the cluster formation in the initial stage of phase decomposition of Al-based alloys, *Metall. Mater. Trans. A*, 34(2003), No. 12, p. 2745.
- [29] A. Biswas, D.J. Siegel, C. Wolverton, and D.N. Seidman, Precipitates in Al–Cu alloys revisited: Atom-probe tomographic experiments and first-principles calculations of compositional evolution and interfacial segregation, *Acta Mater.*, 59(2011), No. 15, p. 6187.
- [30] A. Biswas, D.J. Siegel, and D.N. Seidman, Simultaneous segregation at coherent and semicoherent heterophase interfaces, *Phys. Rev. Lett.*, 105(2010), No. 7, art. No. 076102.
- [31] S.P. Ringer, K. Hono, and T. Sakurai, The effect of trace additions of Sn on precipitation in Al–Cu alloys: An atom probe

- field ion microscopy study, *Metall. Mater. Trans. A*, 26(1995), No. 9, p. 2207.
- [32] D. Mitlin, V. Radmilovic, U. Dahmen, and J.W. Morris, On the influence of Si–Ge additions on the aging response of Al–Cu, *Metall. Mater. Trans. A*, 34(2003), No. 3, p. 735.
- [33] M.P. Moody, A.V. Ceguerra, A.J. Breen, *et al.*, Atomically resolved tomography to directly inform simulations for structure–property relationships, *Nat. Commun.*, 5(2014), art. No. 5501.
- [34] R. Hu, S.B. Jin, and G. Sha, Application of atom probe tomography in understanding high entropy alloys: 3D local chemical compositions in atomic scale analysis, *Prog. Mater. Sci.*, 123(2022), art. No. 100854.
- [35] S. Pogatscher, H. Antrekowitsch, H. Leitner, T. Ebner, and P.J. Uggowitzer, Mechanisms controlling the artificial aging of Al–Mg–Si Alloys, *Acta Mater.*, 59(2011), No. 9, p. 3352.
- [36] S.Q. Zhu, H.C. Shih, X.Y. Cui, C.Y. Yu, and S.P. Ringer, Design of solute clustering during thermomechanical processing of AA6016 Al–Mg–Si alloy, *Acta Mater.*, 203(2021), art. No. 116455.
- [37] X.Z. Wang, D.D. Zhao, Y.J. Xu, and Y.J. Li, Modelling the spatial evolution of excess vacancies and its influence on age hardening behaviors in multicomponent aluminium alloys, *Acta Mater.*, 264(2024), art. No. 119552.
- [38] W.W. Sun, Y.M. Zhu, R. Marceau, *et al.*, Precipitation strengthening of aluminum alloys by room-temperature cyclic plasticity, *Science*, 363(2019), No. 6430, p. 972.
- [39] S.H. Wu, H.S. Soreide, B. Chen, *et al.*, Freezing solute atoms in nanograined aluminum alloys via high-density vacancies, *Nat. Commun.*, 13(2022), No. 1, art. No. 3495.
- [40] S. Pogatscher, H. Antrekowitsch, M. Werinos, *et al.*, Diffusion on demand to control precipitation aging: Application to Al–Mg–Si alloys, *Phys. Rev. Lett.*, 112(2014), No. 22, art. No. 225701.
- [41] R.K.W. Marceau, A. de Vaucorbeil, G. Sha, S.P. Ringer, and W.J. Poole, Analysis of strengthening in AA6111 during the early stages of aging: Atom probe tomography and yield stress modelling, *Acta Mater.*, 61(2013), No. 19, p. 7285.
- [42] P. Dumitraschkewitz, P.J. Uggowitzer, S.S.A. Gerstl, J.F. Löffler, and S. Pogatscher, Size-dependent diffusion controls natural aging in aluminium alloys, *Nat. Commun.*, 10(2019), No. 1, art. No. 4746.
- [43] W. Xu, B. Zhang, X.Y. Li, and K. Lu, Suppressing atomic diffusion with the Schwarz crystal structure in supersaturated Al–Mg alloys, *Science*, 373(2021), No. 6555, p. 683.
- [44] W. Xu, Y.M. Zhong, X.Y. Li, and K. Lu, Stabilizing supersaturation with extreme grain refinement in spinodal aluminum alloys, *Adv. Mater.*, (2023), art. No. 2303650.
- [45] P.N.T. Unwin, G.W. Lorimer, and R.B. Nicholson, The origin of the grain boundary precipitate free zone, *Acta Metall.*, 17(1969), No. 11, p. 1363.
- [46] H. Jiang and R.G. Faulkner, Modelling of grain boundary segregation, precipitation and precipitate-free zones of high strength aluminium alloys—I. The model, *Acta Mater.*, 44(1996), No. 5, p. 1857.
- [47] I.A. Ovid'ko, R.Z. Valiev, and Y.T. Zhu, Review on superior strength and enhanced ductility of metallic nanomaterials, *Prog. Mater. Sci.*, 94(2018), p. 462.
- [48] A.P. Zhilyaev and T.G. Langdon, Using high-pressure torsion for metal processing: Fundamentals and applications, *Prog. Mater. Sci.*, 53(2008), No. 6, p. 893.
- [49] I. Sabirov, M.Y. Murashkin, and R.Z. Valiev, Nanostructured aluminium alloys produced by severe plastic deformation: New horizons in development, *Mater. Sci. Eng. A*, 560(2013), p. 1.
- [50] P.J. Wang, L.W. Ma, X.Q. Cheng, and X.G. Li, Influence of grain refinement on the corrosion behavior of metallic materials: A review, *Int. J. Miner. Metall. Mater.*, 28(2021), No. 7, p. 1112.
- [51] M. Namdar and S.A.J. Jahromi, Influence of ECAP on the fatigue behavior of age-hardenable 2xxx aluminum alloy, *Int. J. Miner. Metall. Mater.*, 22(2015), No. 3, p. 285.
- [52] L. Romero-Reséndiz, A. Flores-Rivera, I.A. Figueroa, *et al.*, Effect of the initial ECAP passes on crystal texture and residual stresses of 5083 aluminum alloy, *Int. J. Miner. Metall. Mater.*, 27(2020), No. 6, p. 801.
- [53] L. Jiang, J.K. Li, G. Liu, *et al.*, Length-scale dependent microalloying effects on precipitation behaviors and mechanical properties of Al–Cu alloys with minor Sc addition, *Mater. Sci. Eng. A*, 637(2015), p. 139.
- [54] Y. Huang, J.D. Robson, and P.B. Prangnell, The Formation of nanograin structures and accelerated room-temperature theta precipitation in a severely deformed Al–4 wt.% Cu alloy, *Acta Mater.*, 58(2010), No. 5, p. 1643.
- [55] A. Deschamps, F. De Geuser, Z. Horita, S. Lee, and G. Renou, Precipitation kinetics in a severely plastically deformed 7075 aluminium alloy, *Acta Mater.*, 66(2014), p. 105.
- [56] T. Hu, K. Ma, T.D. Topping, J.M. Schoenung, and E.J. Lavernia, Precipitation phenomena in an ultrafine-grained Al alloy, *Acta Mater.*, 61(2013), No. 6, p. 2163.
- [57] G. Sha, Y.B. Wang, X.Z. Liao, Z.C. Duan, S.P. Ringer, and T.G. Langdon, Influence of equal-channel angular pressing on precipitation in an Al–Zn–Mg–Cu alloy, *Acta Mater.*, 57(2009), No. 10, p. 3123.
- [58] L. Jiang, J.K. Li, P.M. Cheng, *et al.*, Microalloying ultrafine grained Al alloys with enhanced ductility, *Sci. Rep.*, 4(2014), art. No. 3605.
- [59] J. Royset and N. Ryum, Scandium in aluminium alloys, *Int. Mater. Rev.*, 50(2005), No. 1, p. 19.
- [60] T. Liu, C.N. He, G. Li, X. Meng, C.S. Shi, and N.Q. Zhao, Microstructural evolution in Al–Zn–Mg–Cu–Sc–Zr alloys during short-time homogenization, *Int. J. Miner. Metall. Mater.*, 22(2015), No. 5, p. 516.
- [61] E.A. Marquis and D.N. Seidman, Nanoscale structural evolution of Al₃Sc precipitates in Al(Sc) alloys, *Acta Mater.*, 49(2001), No. 11, p. 1909.
- [62] D.N. Seidman, E.A. Marquis, and D.C. Dunand, Precipitation strengthening at ambient and elevated temperatures of heat-treatable Al(Sc) alloys, *Acta Mater.*, 50(2002), No. 16, p. 4021.
- [63] J. Wadsworth, T.G. Nieh, and J.J. Stephens, Recent advances in aerospace refractory metal alloys, *Int. Mater. Rev.*, 33(1988), No. 1, p. 131.
- [64] K.E. Knipling, R.A. Karnesky, C.P. Lee, D.C. Dunand, and D.N. Seidman, Precipitation evolution in Al–0.1Sc, Al–0.1Zr and Al–0.1Sc–0.1Zr (at.%) alloys during isochronal aging, *Acta Mater.*, 58(2010), No. 15, p. 5184.
- [65] C.B. Fuller, D.N. Seidman, and D.C. Dunand, Mechanical properties of Al(Sc, Zr) alloys at ambient and elevated temperatures, *Acta Mater.*, 51(2003), No. 16, p. 4803.
- [66] C. Booth-Morrison, D.C. Dunand, and D.N. Seidman, Coarsening resistance at 400°C of precipitation-strengthened Al–Zr–Sc–Er alloys, *Acta Mater.*, 59(2011), No. 18, p. 7029.
- [67] M.E. van Dalen, D.N. Seidman, and D.C. Dunand, Creep- and coarsening properties of Al–0.06at.% Sc–0.06at.% Ti at 300–450°C, *Acta Mater.*, 56(2008), No. 16, p. 4369.
- [68] R.D. Li, M.B. Wang, Z.M. Li, P. Cao, T.C. Yuan, and H.B. Zhu, Developing a high-strength Al–Mg–Si–Sc–Zr alloy for selective laser melting: Crack-inhibiting and multiple strengthening mechanisms, *Acta Mater.*, 193(2020), p. 83.
- [69] Q.B. Jia, P. Rometsch, P. Kürsteiner, *et al.*, Selective laser melting of a high strength Al–Mn–Sc alloy: Alloy design and strengthening mechanisms, *Acta Mater.*, 171(2019), p. 108.
- [70] E.A. Marquis, D.N. Seidman, M. Asta, and C. Woodward,

- Composition evolution of nanoscale Al₃Sc precipitates in an Al–Mg–Sc alloy: Experiments and computations, *Acta Mater.*, 54(2006), No. 1, p. 119.
- [71] E.A. Marquis, D.N. Seidman, M. Asta, C. Woodward, and V. Ozoliņš, Mg segregation at Al/Al₃Sc heterophase interfaces on an atomic scale: Experiments and computations, *Phys. Rev. Lett.*, 91(2003), No. 3, art. No. 036101.
- [72] Y. Deng, Z.M. Yin, K. Zhao, J.Q. Duan, J. Hu, and Z.B. He, Effects of Sc and Zr microalloying additions and aging time at 120°C on the corrosion behaviour of an Al–Zn–Mg alloy, *Corros. Sci.*, 65(2012), p. 288.
- [73] Y. Deng, R. Ye, G.F. Xu, et al., Corrosion behaviour and mechanism of new aerospace Al–Zn–Mg alloy friction stir welded joints and the effects of secondary Al₃Sc_xZr_{1-x} nanoparticles, *Corros. Sci.*, 90(2015), p. 359.
- [74] C.Y. Liu, G.B. Teng, Z.Y. Ma, L.L. Wei, B. Zhang, and Y. Chen, Effects of Sc and Zr microalloying on the microstructure and mechanical properties of high Cu content 7xxx Al alloy, *Int. J. Miner. Metall. Mater.*, 26(2019), No. 12, p. 1559.
- [75] S. Bai, X.L. Yi, G.H. Liu, Z.Y. Liu, J. Wang, and J.G. Zhao, Effect of Sc addition on the microstructures and age-hardening behavior of an Al–Cu–Mg–Ag alloy, *Mater. Sci. Eng. A*, 756(2019), p. 258.
- [76] S.Y. Jiang and R.H. Wang, Grain size-dependent Mg/Si ratio effect on the microstructure and mechanical/electrical properties of Al–Mg–Si–Sc alloys, *J. Mater. Sci. Technol.*, 35(2019), No. 7, p. 1354.
- [77] B.A. Chen, L. Pan, R.H. Wang, et al., Effect of solution treatment on precipitation behaviors and age hardening response of Al–Cu alloys with Sc addition, *Mater. Sci. Eng. A*, 530(2011), p. 607.
- [78] B.A. Chen, G. Liu, R.H. Wang, et al., Effect of interfacial solute segregation on ductile fracture of Al–Cu–Sc alloys, *Acta Mater.*, 61(2013), No. 5, p. 1676.
- [79] L. Jiang, J.K. Li, P.M. Cheng, et al., Experiment and modeling of ultrafast precipitation in an ultrafine-grained Al–Cu–Sc alloy, *Mater. Sci. Eng. A*, 607(2014), p. 596.
- [80] S.H. Wu, P. Zhang, D. Shao, et al., Grain size-dependent Sc microalloying effect on the yield strength–pitting corrosion correlation in Al–Cu alloys, *Mater. Sci. Eng. A*, 721(2018), p. 200.
- [81] Y.H. Gao, C. Yang, J.Y. Zhang, et al., Stabilizing nanoprecipitates in Al–Cu alloys for creep resistance at 300°C, *Mater. Res. Lett.*, 7(2019), No. 1, p. 18.
- [82] S. Wu, H. Xue, C. Yang, et al., Hierarchical structure in Al–Cu alloys to promote strength/ductility synergy, *Scripta Mater.*, 202(2021), art. No. 113996.
- [83] J.F. Nie, Physical metallurgy of light alloys, [in] D.E. Laughlin and K. Hono, eds., *Physical Metallurgy*, 5th ed., Elsevier, Amsterdam, 2014, p. 2009.
- [84] J.M. Rosalie and L. Bourgeois, Silver segregation to θ' (Al₂Cu)–Al interfaces in Al–Cu–Ag alloys, *Acta Mater.*, 60(2012), No. 17, p. 6033.
- [85] D. Shin, A. Shyam, S. Lee, Y. Yamamoto, and J.A. Haynes, Solute segregation at the Al/ θ' -Al₂Cu interface in Al–Cu alloys, *Acta Mater.*, 141(2017), p. 327.
- [86] Y.H. Zheng, Y.X. Liu, N. Wilson, et al., Solute segregation induced sandwich structure in Al–Cu (–Au) alloys, *Acta Mater.*, 184(2020), p. 17.
- [87] J.D. Poplawsky, B.K. Milligan, L.F. Allard, et al., The synergistic role of Mn and Zr/Ti in producing θ' /L₁₂ co-precipitates in Al–Cu alloys, *Acta Mater.*, 194(2020), p. 577.
- [88] A.F. Norman, P.B. Prangnell, and R.S. McEwen, The solidification behaviour of dilute aluminium–scandium alloys, *Acta Mater.*, 46(1998), No. 16, p. 5715.
- [89] M.J. Jones and F.J. Humphreys, Interaction of recrystallization and precipitation: The effect of Al₃Sc on the recrystallization behaviour of deformed aluminium, *Acta Mater.*, 51(2003), No. 8, p. 2149.
- [90] M. Ferry and N. Burhan, Structural and kinetic aspects of continuous grain coarsening in a fine-grained Al–0.3Sc alloy, *Acta Mater.*, 55(2007), No. 10, p. 3479.
- [91] J.D.C. Teixeira, D.G. Cram, L. Bourgeois, T.J. Bastow, A.J. Hill, and C.R. Hutchinson, On the strengthening response of aluminum alloys containing shear-resistant plate-shaped precipitates, *Acta Mater.*, 56(2008), No. 20, p. 6109.
- [92] L. Bourgeois, C. Dwyer, M. Weyland, J.F. Nie, and B.C. Muddle, Structure and energetics of the coherent interface between the θ' precipitate phase and aluminium in Al–Cu, *Acta Mater.*, 59(2011), No. 18, p. 7043.
- [93] L. Bourgeois, N.V. Medhekar, A.E. Smith, M. Weyland, J.F. Nie, and C. Dwyer, Efficient atomic-scale kinetics through a complex heterophase interface, *Phys. Rev. Lett.*, 111(2013), No. 4, art. No. 046102.
- [94] C. Yang, P. Zhang, D. Shao, et al., The influence of Sc solute partitioning on the microalloying effect and mechanical properties of Al–Cu alloys with minor Sc addition, *Acta Mater.*, 119(2016), p. 68.
- [95] D.L. Zhang, J. Wang, Y. Kong, Y. Zou, and Y. Du, First-principles investigation on stability and electronic structure of Sc-doped θ' /Al interface in Al–Cu alloys, *Trans. Nonferrous Met. Soc. China*, 31(2021), No. 11, p. 3342.
- [96] K.E. Knippling, D.C. Dunand, and D.N. Seidman, Criteria for developing castable, creep-resistant aluminum-based alloys - A review, *Int. J. Mater. Res.*, 97(2006), No. 3, p. 246.
- [97] S. Jun, Strength for decohesion of spheroidal carbide particle–matrix interface, *Int. J. Fract.*, 44(1990), No. 4, p. R51.
- [98] S.H. Goods and L.M. Brown, Overview No. 1: The nucleation of cavities by plastic deformation, *Acta Metall.*, 27(1979), No. 1, p. 1.
- [99] L.M. Brown and W.M. Stobbs, The work-hardening of copper-silica v. equilibrium plastic relaxation by secondary dislocations, *Philos. Mag.*, 34(1976), No. 3, p. 351.
- [100] T. Marlaud, A. Deschamps, F. Bley, W. Lefebvre, and B. Baroux, Evolution of precipitate microstructures during the retrogression and re-ageing heat treatment of an Al–Zn–Mg–Cu alloy, *Acta Mater.*, 58(2010), No. 14, p. 4814.
- [101] C.R. Hutchinson, X. Fan, S.J. Pennycook, and G.J. Shiflet, On the origin of the high coarsening resistance of Ω plates in Al–Cu–Mg–Ag Alloys, *Acta Mater.*, 49(2001), No. 14, p. 2827.
- [102] Y.H. Gao, P.F. Guan, R. Su, et al., Segregation-sandwiched stable interface suffocates nanoprecipitate coarsening to elevate creep resistance, *Mater. Res. Lett.*, 8(2020), No. 12, p. 446.
- [103] A. Shyam, S. Roy, D. Shin, et al., Elevated temperature microstructural stability in cast AlCuMnZr alloys through solute segregation, *Mater. Sci. Eng. A*, 765(2019), art. No. 138279.
- [104] Y.H. Gao, L.F. Cao, C. Yang, J.Y. Zhang, G. Liu, and J. Sun, Co-stabilization of θ' -Al₂Cu and Al₃Sc precipitates in Sc-microalloyed Al–Cu alloy with enhanced creep resistance, *Mater. Today Nano*, 6(2019), art. No. 100035.
- [105] Y.H. Gao, J. Kuang, J.Y. Zhang, G. Liu, and J. Sun, Tailoring precipitation strategy to optimize microstructural evolution, aging hardening and creep resistance in an Al–Cu–Sc alloy by isochronal aging, *Mater. Sci. Eng. A*, 795(2020), art. No. 139943.
- [106] R. Valiev, Nanostructuring of metals by severe plastic deformation for advanced properties, *Nat. Mater.*, 3(2004), No. 8, p. 511.
- [107] R.Z. Valiev, R.K. Islamgaliev, and I.V. Alexandrov, Bulk nanostructured materials from severe plastic deformation, *Prog. Mater. Sci.*, 45(2000), No. 2, p. 103.
- [108] Y. Estrin and A. Vinogradov, Extreme grain refinement by

- severe plastic deformation: A wealth of challenging science, *Acta Mater.*, 61(2013), No. 3, p. 782.
- [109] A.A. Tiamiyu, E.L. Pang, X. Chen, J.M. LeBeau, K.A. Nelson, and C.A. Schuh, Nanotwinning-assisted dynamic recrystallization at high strains and strain rates, *Nat. Mater.*, 21(2022), No. 7, p. 786.
- [110] K.S. Ghosh, N. Gao, and M.J. Starink, Characterisation of high pressure torsion processed 7150 Al–Zn–Mg–Cu alloy, *Mater. Sci. Eng. A*, 552(2012), p. 164.
- [111] J.G. Brunner, J. May, H.W. Höppel, M. Göken, and S. Virtanen, Localized corrosion of ultrafine-grained Al–Mg model alloys, *Electrochim. Acta*, 55(2010), No. 6, p. 1966.
- [112] E.F. Prados, V.L. Sordi, and M. Ferrante, The effect of Al₂Cu precipitates on the microstructural evolution, tensile strength, ductility and work-hardening behaviour of a Al–4wt.% Cu alloy processed by equal-channel angular pressing, *Acta Mater.*, 61(2013), No. 1, p. 115.
- [113] M. Murayama, Z. Horita, and K. Hono, Microstructure of two-phase Al–1.7 at% Cu alloy deformed by equal-channel angular pressing, *Acta Mater.*, 49(2001), No. 1, p. 21.
- [114] H.L. Jia, R. Bjørge, L.F. Cao, H. Song, K. Marthinsen, and Y.J. Li, Quantifying the grain boundary segregation strengthening induced by post-ECAP aging in an Al–5Cu alloy, *Acta Mater.*, 155(2018), p. 199.
- [115] K. Hockauf, L.W. Meyer, M. Hockauf, and T. Halle, Improvement of strength and ductility for a 6056 aluminum alloy achieved by a combination of equal-channel angular pressing and aging treatment, *J. Mater. Sci.*, 45(2010), No. 17, p. 4754.
- [116] C. Wolverton, Solute–vacancy binding in aluminum, *Acta Mater.*, 55(2007), No. 17, p. 5867.
- [117] J. Peng, S. Bahl, A. Shyam, J.A. Haynes, and D. Shin, Solute–vacancy clustering in aluminum, *Acta Mater.*, 196(2020), p. 747.
- [118] S.K. Kairy, P.A. Rometsch, K. Diao, J.F. Nie, C.H.J. Davies, and N. Birbilis, Exploring the electrochemistry of 6xxx series aluminium alloys as a function of Si to Mg ratio, Cu content, ageing conditions and microstructure, *Electrochim. Acta*, 190(2016), p. 92.
- [119] K.D. Ralston, N. Birbilis, M. Weyland, and C.R. Hutchinson, The effect of precipitate size on the yield strength–pitting corrosion correlation in Al–Cu–Mg alloys, *Acta Mater.*, 58(2010), No. 18, p. 5941.
- [120] M.F. Ashby, Overview No. 80: On the engineering properties of materials, *Acta Metall.*, 37(1989), No. 5, p. 1273.
- [121] E. Ma and T. Zhu, Towards strength–ductility synergy through the design of heterogeneous nanostructures in metals, *Mater. Today*, 20(2017), No. 6, p. 323.
- [122] Y.M. Wang, M.W. Chen, F.H. Zhou, and E. Ma, High tensile ductility in a nanostructured metal, *Nature*, 419(2002), No. 6910, p. 912.
- [123] M. Zha, Y.J. Li, R.H. Mathiesen, R. Bjørge, and H.J. Roven, Microstructure evolution and mechanical behavior of a binary Al–7Mg alloy processed by equal-channel angular pressing, *Acta Mater.*, 84(2015), p. 42.
- [124] Y. Huang and T.G. Langdon, Advances in ultrafine-grained materials, *Mater. Today*, 16(2013), No. 3, p. 85.
- [125] G. Sha, K. Tugcu, X.Z. Liao, *et al.*, Strength, grain refinement and solute nanostructures of an Al–Mg–Si alloy (AA6060) processed by high-pressure torsion, *Acta Mater.*, 63(2014), p. 169.
- [126] Y.D. Zhang, S.B. Jin, P.W. Trimby, *et al.*, Dynamic precipitation, segregation and strengthening of an Al–Zn–Mg–Cu alloy (AA7075) processed by high-pressure torsion, *Acta Mater.*, 162(2019), p. 19.
- [127] Z.Z. Song, R.M. Niu, X.Y. Cui, *et al.*, Room-temperature-deformation-induced chemical short-range ordering in a supersaturated ultrafine-grained Al–Zn alloy, *Scripta Mater.*, 210(2022), art. No. 114423.
- [128] Z.Z. Song, R.M. Niu, X.Y. Cui, *et al.*, Mechanism of room-temperature superplasticity in ultrafine-grained Al–Zn alloys, *Acta Mater.*, 246(2023), art. No. 118671.
- [129] A. Mohammadi, N.A. Enikeev, M.Y. Murashkin, M. Arita, and K. Edalati, Developing age-hardenable Al–Zr alloy by ultra-severe plastic deformation: Significance of supersaturation, segregation and precipitation on hardening and electrical conductivity, *Acta Mater.*, 203(2021), art. No. 116503.
- [130] W. Xu, X.C. Liu, and K. Lu, Strain-induced microstructure refinement in pure Al below 100 nm in size, *Acta Mater.*, 152(2018), p. 138.
- [131] X.Y. Li, Z.H. Jin, X. Zhou, and K. Lu, Constrained minimal-interface structures in polycrystalline copper with extremely fine grains, *Science*, 370(2020), No. 6518, p. 831.
- [132] W. Xu, X.C. Liu, X.Y. Li, and K. Lu, Deformation induced grain boundary segregation in nanolaminated Al–Cu alloy, *Acta Mater.*, 182(2020), p. 207.
- [133] L.H. Su, C. Lu, L.Z. He, *et al.*, Study of vacancy-type defects by positron annihilation in ultrafine-grained aluminum severely deformed at room and cryogenic temperatures, *Acta Mater.*, 60(2012), No. 10, p. 4218.
- [134] J. Čížek, I. Procházka, M. Cieslar, *et al.*, Thermal stability of ultrafine grained copper, *Phys. Rev. B*, 65(2002), No. 9, art. No. 094106.
- [135] X. Sauvage, N. Enikeev, R. Valiev, Y. Nasedkina, and M. Murashkin, Atomic-scale analysis of the segregation and precipitation mechanisms in a severely deformed Al–Mg alloy, *Acta Mater.*, 72(2014), p. 125.
- [136] F.D. Fischer, J. Svoboda, F. Appel, and E. Kozeschnik, Modeling of excess vacancy annihilation at different types of sinks, *Acta Mater.*, 59(2011), No. 9, p. 3463.
- [137] J.Y. Zhang, S. Lei, Y. Liu, *et al.*, Length scale-dependent deformation behavior of nanolayered Cu/Zr micropillars, *Acta Mater.*, 60(2012), p. 1610.
- [138] L.P. Kubin and Y. Estrin, Evolution of dislocation densities and the critical conditions for the Portevin–Le Châtelier effect, *Acta Metall. Mater.*, 38(1990), No. 5, p. 697.
- [139] L.P. Kubin and Y. Estrin, The critical conditions for jerky flow. Discussion and application to CuMn solid solutions, *Phys. Status Solidi B*, 172(1992), No. 1, p. 173.
- [140] X.F. Chen, Q. Wang, Z.Y. Cheng, *et al.*, Direct observation of chemical short-range order in a medium-entropy alloy, *Nature*, 592(2021), No. 7856, p. 712.
- [141] D. Häussler, M. Bartsch, U. Messerschmidt, and B. Reppich, HVTEM *in situ* observations of dislocation motion in the oxide dispersion strengthened superalloy MA 754, *Acta Mater.*, 49(2001), No. 18, p. 3647.
- [142] J. Mola, G.Q. Luan, Q.L. Huang, C. Ullrich, O. Volkova, and Y. Estrin, Dynamic strain aging mechanisms in a metastable austenitic stainless steel, *Acta Mater.*, 212(2021), art. No. 116888.
- [143] R.P. Zhang, S.T. Zhao, J. Ding, *et al.*, Short-range order and its impact on the CrCoNi medium-entropy alloy, *Nature*, 581(2020), No. 7808, p. 283.
- [144] S.H. Jiang, H. Wang, Y. Wu, *et al.*, Ultrastrong steel via minimal lattice misfit and high-density nanoprecipitation, *Nature*, 544(2017), No. 7651, p. 460.
- [145] J.L. Du, S.H. Jiang, P.P. Cao, *et al.*, Superior radiation tolerance via reversible disordering–ordering transition of coherent superlattices, *Nat. Mater.*, 22(2023), No. 4, p. 442.